ATTENUATION BASED QUANTIFICATION OF INTERSTITIAL LUNG DISEASE USING HIGH RESOLUTION COMPUTED TOMOGRAPHY AND CORRELATION WITH PULMONARY FUNCTION TESTS

by

SNEHAL S WATHARKAR

Presented to the Faculty of the Graduate School of

The University of Texas at Arlington in Partial Fulfillment

Of the Requirements

For the Degree of

MASTER OF SCIENCE IN BIOMEDICAL ENGINEERING

THE UNIVERSITY OF TEXAS AT ARLINGTON

AUGUST 2010

ACKNOWLEDGEMENTS

First and foremost, I want to express my sincere gratitude towards Dr Connie Hsia for her guidance and support from the initial to final level, which enabled me to develop an understanding of the subject. Besides my advisor I would like to thank Dr Hanli Liu and Dr George Alexandrakis for serving on my committee and providing valuable comments on my work.

I would like to thank Dr Cuneyt Yilmaz for his constant help and support in every aspect of my research work. I would also like to thank Dr Nova Patel for her advice on image interpretation and guidance on fissure detection. I am most grateful to Dr Priya Ravikumar and other laboratory staff for their good advice; support and friendship.

Above all I am indebted to my parents: Subhash Watharkar and Madhuri Watharkar and my fiancé Kedar Karandikar for their unconditional support and encouragement to pursue my interests. I am grateful to my close friends for their strong encouragement, patience and listening to me and believing in me and my work.

June 11, 2010

ABSTRACT

ATTENUATION BASED QUANTIFICATION OF INTERSTITIAL LUNG DISEASE USING HIGH RESOLUTION COMPUTED TOMOGRAPHY AND CORRELATION WITH PULMONARY FUNCTION TESTS

Snehal S. Watharkar M.S.

The University of Texas at Arlington, 2010

Supervising Professor: Connie Hsia.

Interstitial lung disease (ILD) is a chronic and progressive pulmonary disease of the lung parenchyma resulting in fibrotic scar formation of the pulmonary alveoli. The pathologic changes in the lung result in restrictive impairment of lung function. High resolution computed tomography (HRCT) of the chest has become an essential technique in diagnosing and assessing the extent of ILD. Clinical evaluation by HRCT is usually qualitative, leading to inter-observer variability particularly in detecting early disease. We propose a quantitative attenuation-based analysis to standardize the assessment of regional lung disease. We hypothesize that early ILD is associated with greater regional heterogeneity than advanced ILD. To test the hypothesis a method of voxel-wise HRCT image analysis is used to quantify regional lung tissue and air volume within and among lobes.

We analyzed HRCT (0.625mm intervals from apex to base) obtained at prone end-inspiration, supine end-inspiration and supine end-expiration in 29 patients with ILD. Each

lobe was reconstructed separately. Regional air and tissue volumes, and fractional tissue volume (FTV=tissue/ [air + tissue] volume) were expressed along standard x,y,z axes. FTV increased with increasing ILD severity especially in the periphery. Lobar FTV correlates inversely with global lung function in all lobes. Early ILD is associated with greater FTV heterogeneity within lobes. With increasing ILD severity, FTV heterogeneity within lobes decreases while FTV heterogeneity among lobes increases.

We conclude that quantitative analysis of FTV can provide clinically relevant markers of regional ILD. ILD severity is associated with decreasing intra-lobar and increasing inter-lobar FTV heterogeneity, best assessed at prone end-inspiration.

TABLE OF CONTENTS

LIST OF ILLUSTRATIONS

Figure Page

LIST OF TABLES

CHAPTER 1

INTRODUCTION

1.1 Normal lung anatomy and function

1.1.1 Organ of Respiration

The thoracic cage is bounded by the bones of spine and rib cage with the intercostal muscles and diaphragm. The thoracic cage contains the lungs, airways, tracheobronchial tree, the heart and the vessels transporting the blood between the heart and lungs. The lung is separated into lobes by inter-lobar fissures [Fig 1.1]. The lungs bring oxygen into the body and removes carbon dioxide from the body. Air breathed through the nose and mouth passes through the trachea into the lungs. The trachea branches into successive generations of bronchi, eventually entering the terminal bronchioles. The terminal bronchioles further branch into respiratory bronchioles and alveolar ducts to carry oxygen to more than 300 millions of alveoli [Fig 1.2]. [1].

Respiration involves two sets of muscles that change the volume of the thoracic cavity to generate inspiration and expiration. The two sets of muscles involved are the diaphragm and the intercostal muscles [2]. Inspiration results from downward movement of diaphragm and up and outward movement of the ribcage. Expiration results from passive upward movement of diaphragm and inward and downward movement of the rib cage.

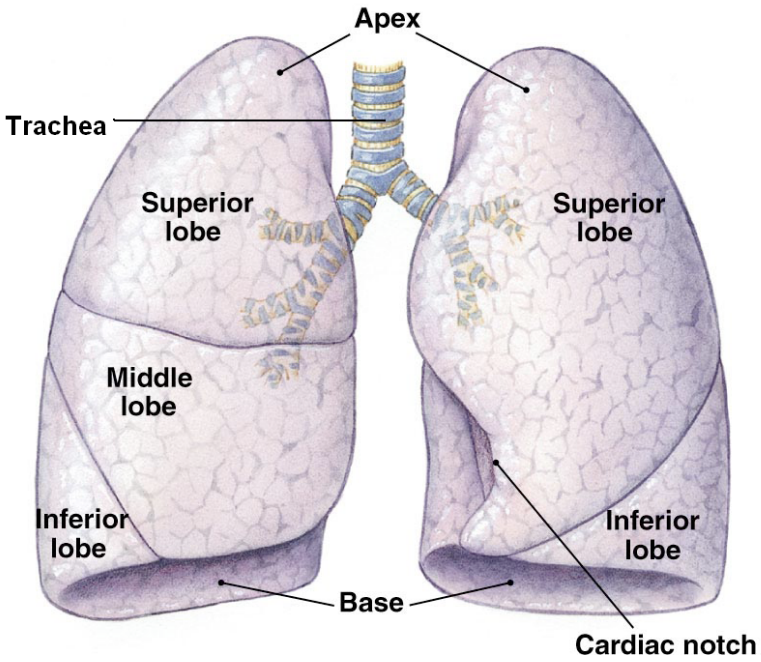

Figure 1.1 Lung anatomy. [2]

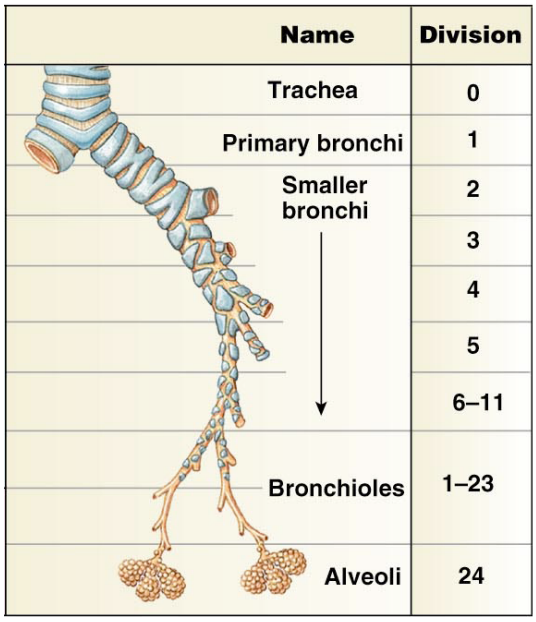

Figure 1.2 Airway branching in human lung [2].

1.1.2 Pulmonary function parameters

The pulmonary function tests are measurements that indicate the state of respiratory function that includes lung volumes and capacities, airway resistance, lung compliance and elasticity. Lung volume is the amount of air the lung can hold while lung capacities are the combinations of two or more lung volumes [Figure 1.3]. Pulmonary function tests are often used to diagnose and follow clinical diseases. The measurements of lung volumes and the rate of air movement are important tools in assessing the health and breathing capacities of a person.

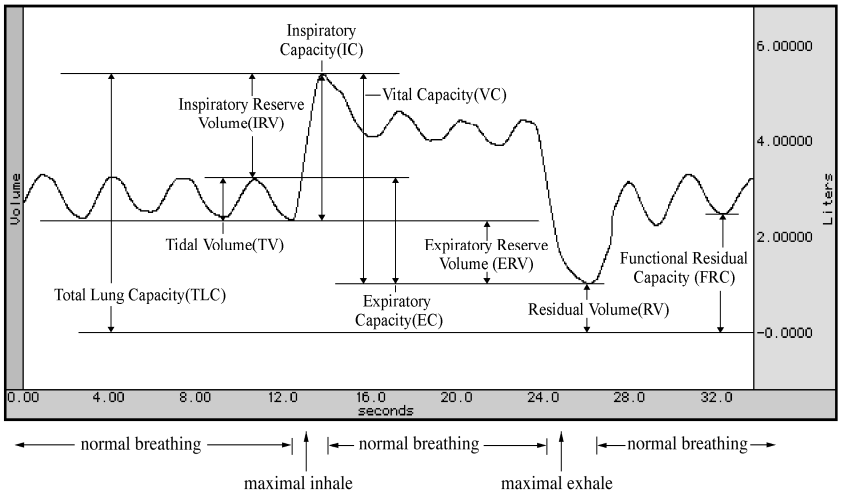

Figure 1.3 Pulmonary volume and capacities. [3]

1.2 Interstitial Lung Disease (ILD)

1.2.1 Background of Interstitial lung disease (ILD)

Interstitial lung disease (ILD) is a chronic and progressive inflammatory disease of the lung parenchyma resulting in fibrotic scar formation of the pulmonary alveoli. ILD is a general term that includes many disorders that are categorized by interstitial pneumonitis. The known causes of interstitial pneumonitis include drugs, viral infection, malignancy and immunological

reaction to inhaled organic or inorganic antigens. If of unknown origin they are classified as idiopathic interstitial pneumonitis. Based on morphological characteristics, idiopathic interstitial pneumonitis can be classified as usual interstitial pneumonia, idiopathic pulmonary fibrosis, desquamative interstitial pneumonia, nonspecific interstitial pneumonia, or acute interstitial pneumonia [4] [5].

In the early stages of ILD, inflammation of the air sacs develops. Progressive tissue damage eventually leads to scar formation and obliteration of capillaries that impair oxygen diffusion into the blood. Symptoms of ILD include dry cough and dyspnea [6]. These pathologic abnormalities can lead to impairment of lung function. It is very important to define the extent of disease activity in ILD patients in order to adjust medication and assess treatment response.

1.2.2 Pulmonary function tests

Pulmonary function tests are routinely used in the management of patients with ILD. They are useful in diagnosing disease, defining prognosis, and determining disease progression and response to therapy. Physiologic testing commonly includes spirometry: forced expiratory volume in 1 second (FEV_1) forced vital capacity (FVC), and lung diffusing capacity for carbon dioxide (DL_{CO}). The pathologic changes in the lung (inflammation and fibrosis) result in restriction of lung function whereby both FEV_1 and FVC are proportionately reduced. [7].

1) FVC: It is the volume of air that is exhaled forcefully following a maximum inhalation effort. FVC is measured in liters.
2) FEV_1: It is the maximal amount of air that can be forcibly exhaled in the first second during the forced expiration maneuver. The unit of measurement of FEV_1 is liters. FEV_1 is a measure of the flow rate of large airways.

3) DL_{CO}: It is the measurement of carbon monoxide (CO) transfer from inspired gas to pulmonary capillary blood. [8]. The unit for DL_{CO} is mL [min .mmHg]$^{-1}$. DL_{CO} is a measure of the gas exchange capacity of lungs.

1.3 Imaging techniques for ILD

1.3.1 Chest radiographs

The chest radiograph is the traditional technique used in evaluating the severity of lung disease. Typical radiographic findings in patients with ILD include reduced lung volumes and increased interstitial opacities. However, there are a few concerns regarding the reproducibility and sensitivity of this diagnostic method. The chest radiographs in early idiopathic pulmonary fibrosis are often normal making it insensitive for detection of early parenchymal diseases.

1.3.2 High resolution computed tomography (HRCT)

The development of HRCT led to more precise anatomic definition of interstitial lung disease. Hence more information is available than the traditional diagnostic tools like chest radiographs and standard CT to assess the extent of pulmonary fibrosis.

1.4 Technical aspects of HRCT

1.4.1. Basic Principles

Computed tomography is a radiological modality that produces cross sectional anatomical images. In these images, the value of each pixel corresponds to the X-ray attenuation of a defined volume (voxel) of tissue. Different substances and tissues differ in their ability to absorb x-rays. Owing to this difference, dense tissues such as the bones appear white on a CT

film while the soft tissues such as the brain or kidney appear gray. The cavities filled with air such as the lungs appear black.

The CT image consists of 512x512 pixels representing the CT number, which is expressed in Hounsfield unit (HU). CT number is defined as:

$$\text{CT number (in HU)} = \frac{\mu - \mu_{water}}{\mu_{water}} \times 1000$$

Where μ = linear attenuation coefficient and μ_{water} is the linear attenuation coefficient of water. With this definition air, water and bone have CT number of, -1000HU, 0 HU, and 1000 HU respectively. Soft tissues have CT value between -100HU to 60HU [9] [10].

1.4.2 Components of HRCT

The main components of a CT scanner are: x-ray tube and array of detectors opposite to the tube. The number and geometry of the detectors are variable [Fig 1.5]. The basic working principle is passing x-rays through the patient and obtaining information with a detector on the other side. The x-ray source and the detector are interconnected and rotated around the patient during scanning period. Once the scan is initiated the operational control computer instructs the gantry to rotate to the desired position as instructed by the operator. The computer then sends signal to the patient table, the x-ray generation system, the x-ray detection system and to the image generation system. The high voltage generator maintains the voltage and current to the x-ray tube at the prescribed level during the scan. The x-ray tube produces x-ray photons that are detected by the x-ray detector. The signal from the x-ray detectors is reconstructed by a computer, to provide a cross sectional image (tomogram) that is displayed on a computer screen [11].

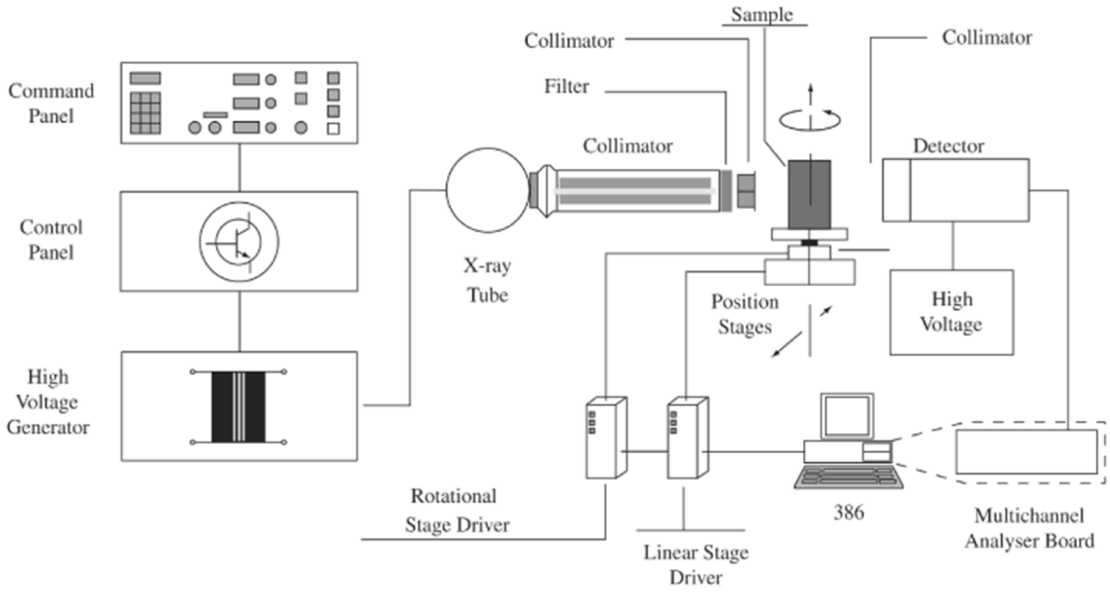

Figure 1.4 Block Diagram of CT scanner[12].

1.4.3 Technical Parameters

1) Tube voltage and tube current: X-ray tubes supply the necessary photons to perform a scan. Since the intensity of the x-ray radiation is proportional to the number of impacting electrons, it is essential to control tube current and voltage. The recommended setting to get optimal HRCT images for tube voltage are 120-140 kV (p) and for tube current are 240 mA.

2) Spatial resolution: Spatial resolution is measured by the ability of a CT system to distinguish small structures from each other. The reconstructed image should have a high spatial resolution to improve image quality. The maximum spatial resolution can be determined by the spatial frequency at which the scan data are sampled during the scan sequence. Reconstruction of the image using high spatial frequency algorithm increases the spatial resolution.

3) Collimation: Collimation describes how thick or thin the acquired slices can be, along the longitudinal axis (z-axis) of the patient. The examiner can limit the fan-like x-ray tube by a collimator, while collimator's aperture determines whether the fan passing through the

collimator at the detector unit is narrow or wide. Thin collimation allows a better spatial resolution along the z-axis. The collimation used is typically in the range of 1.0-1.5 mm.

4) Pitch: Pitch is defined as the table travel per gantry rotation and selected collimation.

$$\text{Pitch} = \frac{\text{table travel/rotation}}{\text{Collimation}}$$

Higher pitch increases the volume coverage. The recommended pitch setting for HRCT is in the range of 0.5 to 2.0.

5) Scan Time: Scan time of 1 second or less is recommended for HRCT. Because of patient motion, longer scan time can result in motion related artifacts [13].

1.5 Volumetric HRCT

Volumetric HRCT can be performed using various techniques including conventional HRCT with contiguous slices, single detector-row or multi-detector-row spiral CT. Spiral or helical CT is a technique which is widely spread nowadays. In this technique the x-ray tube rotates around the patients and at the same time the patient is translated through the gantry at a constant rate and the data is acquired. Volumetric reconstruction of scan data is possible in each of these techniques. Volumetric HRCT has various advantages over standard CT 1) complete imaging of the lung is possible 2) a better understanding of the lung abnormalities in 3D distribution 3) Viewing of contiguous slices for better definition of lung abnormalities [14].Fig 1.5 illustrates increased spatial resolution of HRCT as compared to standard CT. [15].

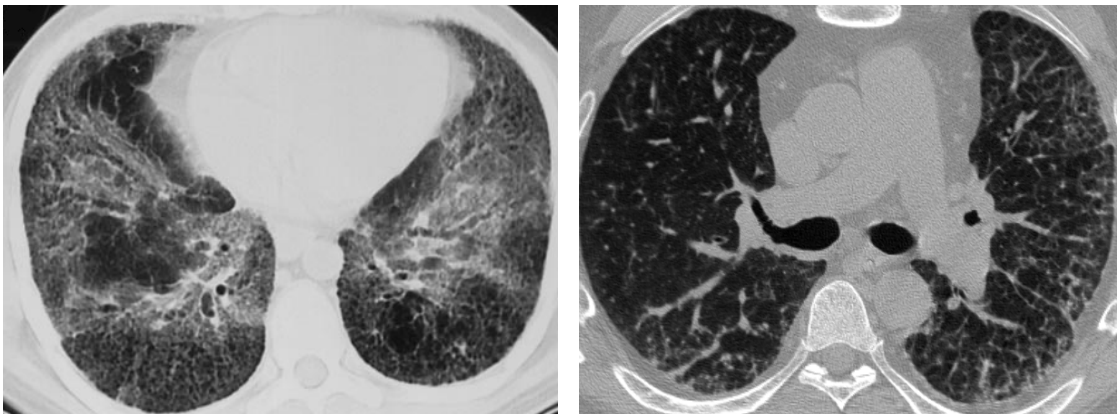

(a) (b)

Figure 1.5. Increased spatial resolution in (a) HRCT scan compared to (b) standard CT [16]

1.5.1 Single –detector row spiral computed tomography

Single detector row spiral CT scanners have the ability to obtain volumetric CT data, with a 1-2 cm slice thickness of lung during single breath hold. Because the limited amount of lung is assessed during single breath hold this technique has limited applications.

1.5.2 Multi-detector row spiral computed tomography

Multi-detector row spiral computed tomography makes use of multiple detector rows that can be used independently or in combination to generate images of different thickness. This shortens the imaging time and improves the spatial resolution. The scanners are capable of imaging the entire thorax within 7-10 seconds in a single breath hold. [Figure 1.7]

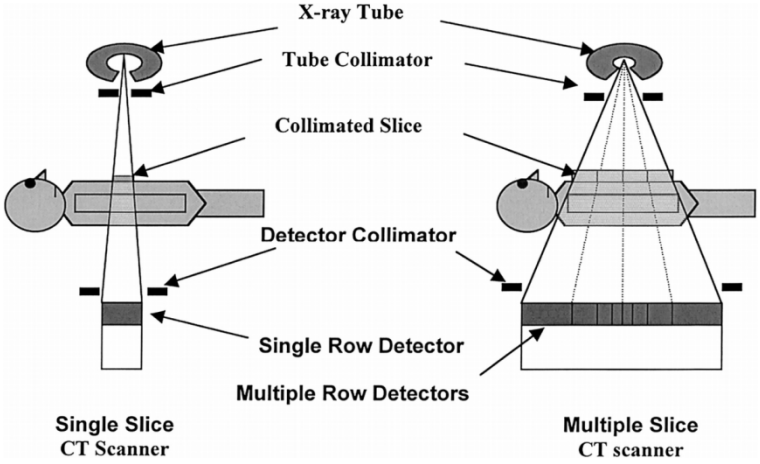

Figure 1.6 Single detector row and multi-detector row spiral CT [17].

1.6 Role of HRCT in imaging of ILD

Currently HRCT is routinely used to qualitatively evaluate the extent of disease. The correlation between HRCT appearances and pulmonary abnormalities allow accurate anatomic terms to be used in describing patterns of interstitial lung disease. The abnormalities of the lung parenchyma on HRCT can be classified into four patterns: 1) reticular and linear opacities, 2) nodular opacities 3) ground-glass attenuation and 4) cystic air spaces [18]. These terms are defined in Table 1.1.

Table 1.1 HRCT terms

Term	Definition
Reticulation	Innumerable, interlacing small linear opacities that suggest a mesh.
Irregular linear opacities	Linear opacity of irregular thickness of 1-3 mm.
Nodular opacity	Round opacity, no greater than 3cm in diameter.
Ground glass attenuation	Hazy increased attenuation of the lung that did not obscure underlying vessels.
Cystic Airspaces	Round airspaces with well-defined wall.

Visual scoring systems are used to evaluate the extent of disease on CT using the above defined anatomical terms. The visual scoring systems are subjective and are limited by the

requirement of radiological expertise [19]. Hence there is an increasing need for development of a quantitative, non-invasive and reproducible technique. Quantitative analysis of lung abnormalities is an attempt to take advantage of the large quantity of digital data that is collected by the CT scanning process.

1.7 Objective of Study

In this study the CT dataset is analyzed in an objective and quantitative manner to fully utilize the information content from the CT images. The overall goal was to improve the detection of early parenchymal lung disease through objective quantification of regional abnormalities on HRCT that maximally utilize each HRCT dataset. I quantified regional CT attenuation in patients with ILD to test the hypothesis that regional heterogeneity is a hallmark of early ILD. A method of voxel-wise HRCT image analysis, developed by Dr. Cuneyt Yilmaz was applied to quantify regional lung tissue and air volume along standard x,y,z-axes within and among lobes [20] [21] [22]. The main objectives of this study are: 1) to quantify and map regional distributions of air and tissue within and among lobes for patients with ILD 2) to correlate CT-derived parameters with lung function 3) to correlate the heterogeneity of tissue distribution with ILD severity.

CHAPTER 2

METHODS AND MATERIALS

2.1 Patient groups

2.1.1 Source of data

The patient data and HRCT images were obtained from the Lung Tissue Research Consortium (LTRC). The LTRC is a research program sponsored by National Heart Lung and Blood Institute (NHLBI). The LTRC collects human lung tissues, imaging and clinical data from designated centers for research purposes and provides these to qualified and approved investigators. The data is collected from four clinical centers: The Mayo clinic, University of Colorado, University of Michigan and University of Pittsburgh. The donor subjects are enrolled in the program; the subjects have interstitial lung disease or COPD. Phenotypic data, blood and tissue samples are collected from the donor subjects who are anticipating lung surgery. Phenotypic data include clinical and pathological diagnoses, chest CT images, pulmonary function tests, exposure and symptom questionnaires, and exercise tests [23].

2.1.2 Patient data

The LTRC protocol for HRCT consists of three helically acquired data sets on a multi-detector CT scanner (with no less than 8 detectors) with tube voltage of 140 kVp and tube current of 324 mA. Scans were optimized to allow for single breath acquisition in less than 15 seconds .CT data of 29 patients (13 females and 16 men, age 26-78 yrs) with ILD was obtained at supine end-inspiration, supine end-expiration and prone end-inspiration positions. The CT

images were reconstructed at consecutive 0.625 mm intervals from apex to base resulting in ~ 400 images per patient. The patients were classified according to the disease severity – mild, moderate, severe, more severe ILD. The patients are classified according to their FVC (% predicted values). Group1- Mild ILD: >=80%; Group 2- Moderate ILD: 50-80%; Group 3- Severe ILD: 30-50%; and Group 4- More Severe ILD: <30%. Demographic data include patient sex, age, pulmonary function tests- FEV_1 and FVC, DL_{CO}.

Table 2.1 describes the demographic data and lung function. The demographic data for ILD patients in 4 groups include: number of patients in each group, age, gender, height, weight, body mass index (BMI), and hemoglobin. The lung function data include absolute and % predicted values for FEV_1 and FVC, DL_{CO} and FEV_1/FVC % predicted. In ILD inspiration is limited by decreased lung compliance which results in normal to increased air flow. The FEV_1 and FVC are reduced proportionately. Due to alveolar fibrosis DL_{CO} is also reduced. The reduction in lung function parameters with increasing disease severity can be seen in the table. The absolute and % predicted values for FEV_1 and FVC, DL_{CO} are reduced with increasing disease severity. The FEV_1/FVC ratio is a good index for distinguishing obstructive from restrictive pathophysiology. The FEV_1/FVC is typically normal in restrictive diseases while it is reduced in obstructive diseases. Because ILD is a restrictive disease the FEV_1/FVC ratio remains almost constant with increasing disease severity as FEV_1 and FVC are proportionately reduced as shown in table 2.1.

Table 2.1 Demographic data and lung function

	ILD Severity			
	Mild	Moderate	Severe	More Severe
n	7	11	9	2
Males	3	7	6	0
Females	4	4	3	2
Age,yrs	64±9	57±15	55±6	40±19
Height, cm	167± 9	169±8	168±10	167±3
Weight,kg	82±12	87±16	79±17	65±22
BMI, $kg.m^{-2}$	42.6±3.6	43.4±4.1	41.7±4.1	37.5±8.0
Hemoglobin, $g.dL^{-1}$	14.4±1.4	14.7±1.2	13.2±1.8	13.0
Pulmonary function tests				
FEV_1, L	2.64±0.50	2.15±0.49	1.44±0.40	1.00±0.14
FEV_1, % predicted	95±7	70±14	44±8	31±1.40
FVC, L	3.40±0.80	2.70±0.67	1.79±0.40	1.05±0.07
FVC, % predicted	88±10	66±10	42±6	44±8
FEV_1/FVC, % predicted	109.18±10.05	106±11.30	106.36±12.15	119.26±1.05
DL_{CO}, $ml[min.mmHg]^{-1}$	15±5	10±4	7.50±3	_
DL_{CO}, % predicted	80±27	44±22	31±8	_

Mean±SD.

2.2 Data analysis

2.2.1 Semi-Automatic method of lobar partition

Images in DICOM format were transferred from the LTRC to a personal computer and analyzed using a semi-automatic image analysis program that was developed in our laboratory by Dr. Yilmaz using Visual C++ 6.0 with OpenGL library. The area occupied by lung tissue on each image was outlined by density thresholding. The trachea and next three generations of large airways and blood vessels were excluded manually.

A semi-automatic image analysis program was used to separate individual lobes by lobar fissures. To identify individual lobes, the fissures were fitted with cubic splines interpolation on all images. On the 1st image the fissure was manually selected and marked by points. Then program automatically detects this fissure line by plotting cubic splines between the first and last point. 10 images ahead, again the first and last point of the fissure was marked by points. Again the program automatically detects this fissure line by plotting cubic splines between the first and last point on the 10th image.

Fissures were identified manually every 10 images and fitted with cubic splines. Similar fissure detection was done every 10 images and fissures in between these images were identified by linear interpolation. The technique of interpolation was used to estimate the fissure lines on the images between the 1st and the 10th image. If required the images were revisited and the splines on the fissures manually corrected.

The right lung consists of 3 lobes- right upper lobe (RUL), right middle lobe (RML) and right lower lobe (RLL). The left lobe lung consists of 2 lobes- left upper lobe (LUL including the lingula) and left lower lobe (LLL). Figure 2.1 illustrates the detected fissures in both the right and left lungs separating the right lung into 3 lobes: RUL, RML and RLL, and the left lung into 2 lobes: LUL (including the lingula) and LLL. Lung volume in each image is the

product of its area and slice thickness. Figure 2.2 shows the area selection of LUL. Similar area selection is done for all the images and each lobe is reconstructed separately [20] [21]. Figure 2.3 illustrates the three dimensional reconstruction at supine end-inspiration in a patient with mild ILD. The left upper panel illustrates the posterior view of the lungs; the left lower panel illustrates the oblique caudal view of the lungs. The right upper panel and right lower panel show the three-dimensional reconstruction of the airways in posterior and oblique caudal views, respectively.

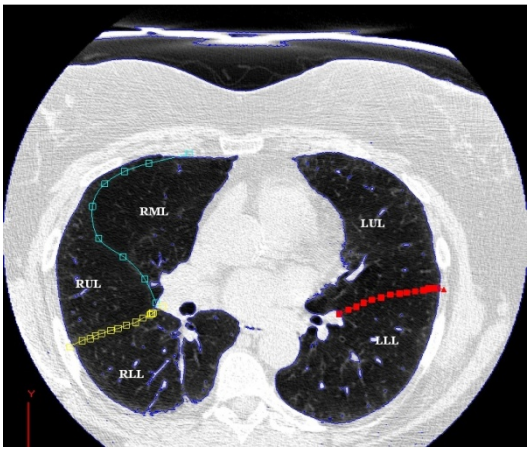

Figure 2.1. Detected fissures in the lung.

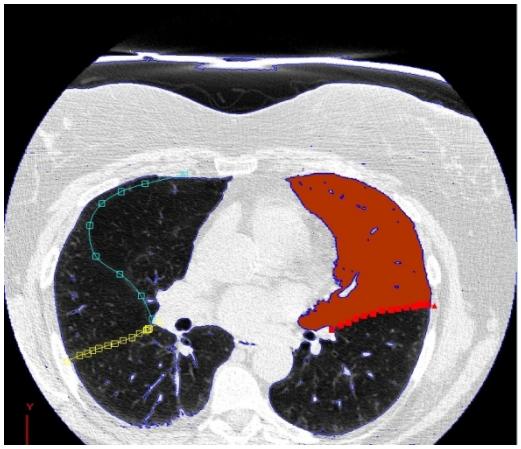

Figure 2.2 Area selection for LUL

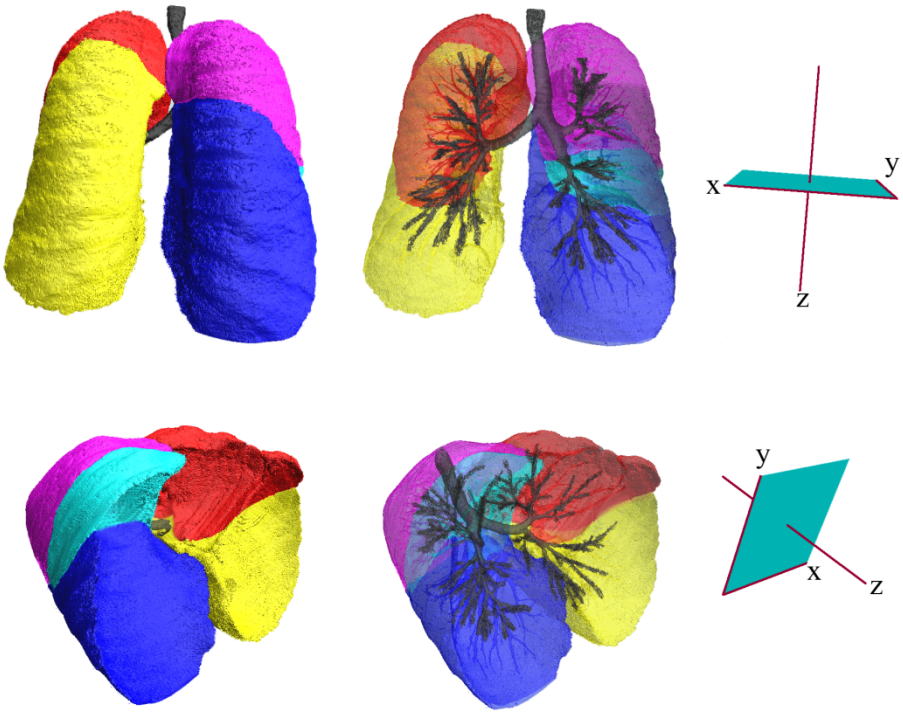

Figure 2.3 Three-Dimensional reconstructions at supine end-inspiration in a patient with mild ILD in posterior view (left upper panel) and oblique caudal view (left lower panel). The color scheme is as follows: pink for RUL, sky blue for RML, navy blue for RLL, red for LUL and yellow for LLL.

2.2.2 Calculating Air volume, Tissue volume and FTV

The CT attenuation of extra-thoracic air was set at -1000 HU and that of water at 0 HU. The CT densities in (HU) of tracheal air and skeletal muscle were directly measured from the CT images as estimates for air and tissue density respectively. The CT attenuation for tracheal air was calculated from averaging 3 different points 5 mm above carina. The value calculated for air density was in the range of +65 to +75 HU. Assuming the average CT value for air-free lung tissue equals that of muscle we averaged 3 muscles in infraspinatus, supraspinatus and pectoralis at the level just above the carina. The value calculated was in the range of -1090 to -1100 HU. These values of air density and muscle density were used to partition the total lobar

volume into air volume and tissue volume. Lobar tissue and air volume were calculated as below:

$$\text{Lobar tissue volume} = \frac{\text{lobar density} - \text{air density}}{\text{muscle density} - \text{air density}} \times \text{lobar volume}$$

$$\text{Lobar air volume} = \text{total volume} - \text{tissue volume}$$

$$\text{Fractional Tissue Volume(FTV)} = \frac{\text{tissue volume}}{\text{lobar volume}}$$

2.2.3 Validating the analysis of gap images

Out of a total of 29 sets of images, 15 sets were analyzed exhaustively, i.e., ~400 consecutive images 0.625 mm apart. In the remaining 14 sets, every 10th consecutive images were analyzed, i.e., ~40 images 6.25 mm apart. We validated the latter method against the former in 4 patients. The percentage differences between the two methods for air volume (Vair) was calculated for the RUL, RML, RLL, LUL, LLL, right lung, left lung and total lungs in 3 positions for 4 patients as follows:

$$\text{Difference} = \frac{\text{Vair (6.25mm)} - \text{Vair (0.625mm)}}{\text{Vair (0.625mm)}} \text{X } 100$$

Similarly the percentage difference was calculated for tissue volume and FTV. Table 2.2 summarizes the minimum and maximum range of percentage difference for every 0.625 mm and 6.25 mm in RUL, RML, RLL, LUL, LLL, right lung, left lung and total lungs in 3 positions for 4 patients. The minimum percentage difference is 0.01% and maximum is 3%; hence the error for values of the CT derived parameters: air volume, tissue volume and FTV, at every 0.625 mm and 6.25 mm slice apart is small. We conclude that the HRCT and analysis in ILD can be performed at larger intervals, which could minimize the total radiation exposure during scan.

Table 2.2 Summary of percentage difference in air volume, tissue volume and FTV for analysis using all consecutive images (0.625 mm thickness) and gap images (0.625 mm thickness every 6.25 mm apart).

Sup-Insp (n=4)	**Air Volume**			**Tissue Volume**			**FTV**		
	Min		Max	Min		Max	Min		Max
Right Upper Lobe	0.598	-	0.148	0.081	-	1.396	0.003	-	0.880
Right Middle Lobe	0.606	-	0.361	1.064	-	0.718	0.390	-	0.309
Right Lower Lobe	0.288	-	0.228	0.044	-	1.019	0.052	-	1.000
Left Upper Lobe	0.091	-	0.022	0.306	-	0.664	0.211	-	0.624
Left Lower Lobe	0.030	-	0.098	0.518	-	0.105	0.489	-	0.010
Right Lung	0.227	-	0.143	0.161	-	0.803	0.048	-	0.518
Left Lung	0.020	-	0.048	0.228	-	0.029	0.159	-	0.023
Total Lungs	0.119	-	0.046	0.075	-	0.293	0.036	-	0.293
Sup-Exp (n=4)	**Air Volume**			**Tissue Volume**			**FTV**		
Right Upper Lobe	0.511	-	0.479	0.617	-	0.004	0.757	-	0.013
Right Middle Lobe	0.529	-	0.047	1.004	-	1.001	0.561	-	1.231
Right Lower Lobe	0.128	-	0.714	1.567	-	0.110	0.942	-	0.120
Left Upper Lobe	0.120	-	0.684	0.488	-	1.196	0.292	-	0.330
Left Lower Lobe	0.014	-	0.181	0.462	-	0.221	0.304	-	0.139
Right Lung	0.156	-	0.267	1.027	-	0.202	0.538	-	0.048
Left Lung	0.083	-	0.409	0.226	-	0.198	0.123	-	0.136
Total Lungs	0.122	-	0.176	0.383	-	0.074	0.325	-	0.061
Prone-Insp (n=4)	**Air Volume**			**Tissue Volume**			**FTV**		
Right Upper Lobe	0.022	-	0.156	1.658	-	0.188	1.181	-	0.080
Right Middle Lobe	1.284	-	1.767	1.772	-	3.007	0.439	-	1.009
Right Lower Lobe	0.012	-	0.799	0.127	-	2.121	0.101	-	0.932
Left Upper Lobe	0.141	-	0.227	0.239	-	0.167	0.252	-	0.051
Left Lower Lobe	0.129	-	0.111	0.354	-	0.435	0.245	-	0.499
Right Lung	0.083	-	0.491	0.120	-	0.722	0.150	-	0.193
Left Lung	0.107	-	0.034	0.303	-	0.199	0.227	-	0.272
Total Lungs	0.094	-	0.214	0.133	-	0.363	0.146	-	0.169

2.2.4 Regional Analysis of Air volume, Tissue volume and FTV

Regional FTV gradients were calculated along the three coordinate axes: x (medial-to-lateral), y (posterior-to-anterior) and z (cephalad-to-caudal). Each axis is classified into bins: 0-10%, 10-30%, 30-50%, 50-70%, 70-90% and 90-100%, of total span and analyzed with respect to average position of the bin along a given axis i.e. 5, 20,40,60, 80 and 95%.

The coefficient of variation (CV = SD/mean) in FTV was calculated within and among lobes to assess heterogeneity. CV among lobes was calculated to determine inter-lobar heterogeneity. CV within lobes and among bins, for each coordinate axes was calculated to determine intra-lobar heterogeneity. Calculated inter-lobar and intra-lobar CV's are correlated with PFT.

2.2.5 Statistical Analysis

Measurements were expressed as mean ± SD. Comparisons for air volume; tissue volume and FTV for 3 positions within disease groups were performed using factorial ANOVA by Fishers protected least significant difference. Correlation between inter-lobar and intra-lobar CV with PFT were performed by simple regression analysis. We used a commercial statistical package STATVIEW (v.5.0, SAS Institute, Cary, NC). A p value ≤ 0.05 was considered significant.

CHAPTER 3

RESULTS

3.1 Qualitative analysis of CT

Figure 3.1 shows examples of axial cross section HRCT images for (a) mild, (b) moderate, (c) severe and more (d) severe ILD. ILD is associated with patchy and inhomogeneous tissue distribution. With increasing disease severity there is an increase in patchy areas of high attenuation in both lungs. This is illustrated in the Figure 3.2; the same HRCT images are shown in cross-sectional color maps of FTV for (a) mild, (b) moderate, (c) severe and more (d) severe ILD. Patchy areas in HRCT scans can be compared with the high FTV regions in the color maps which show the increase in FTV with increasing disease severity. Regions of higher FTV are depicted by yellow and red colors. Figure 3.3 illustrates the three-dimensional surface color maps of FTV for (a) mild, (b) moderate, (c) severe and more (d) severe ILD. In early ILD i.e. at mild and moderate disease stage, the patchy areas of high FTV are seen at lower lobes and especially at the periphery. But with increasing disease severity the middle and upper lobes are also affected.

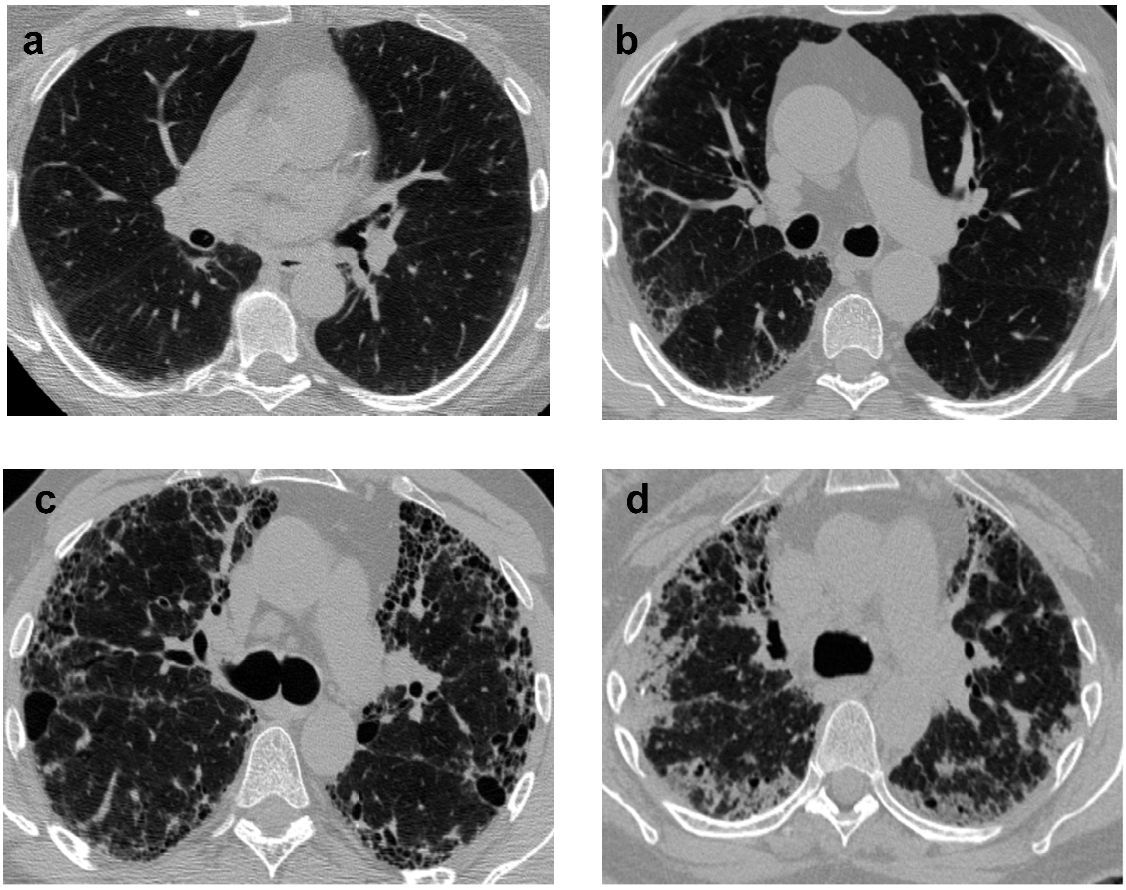

Figure 3.1 Sample HRCT images for (a) mild, (b) moderate, (c) severe and more (d) severe ILD. With increasing disease severity there is an increase in patchy areas of high attenuation in both lungs.

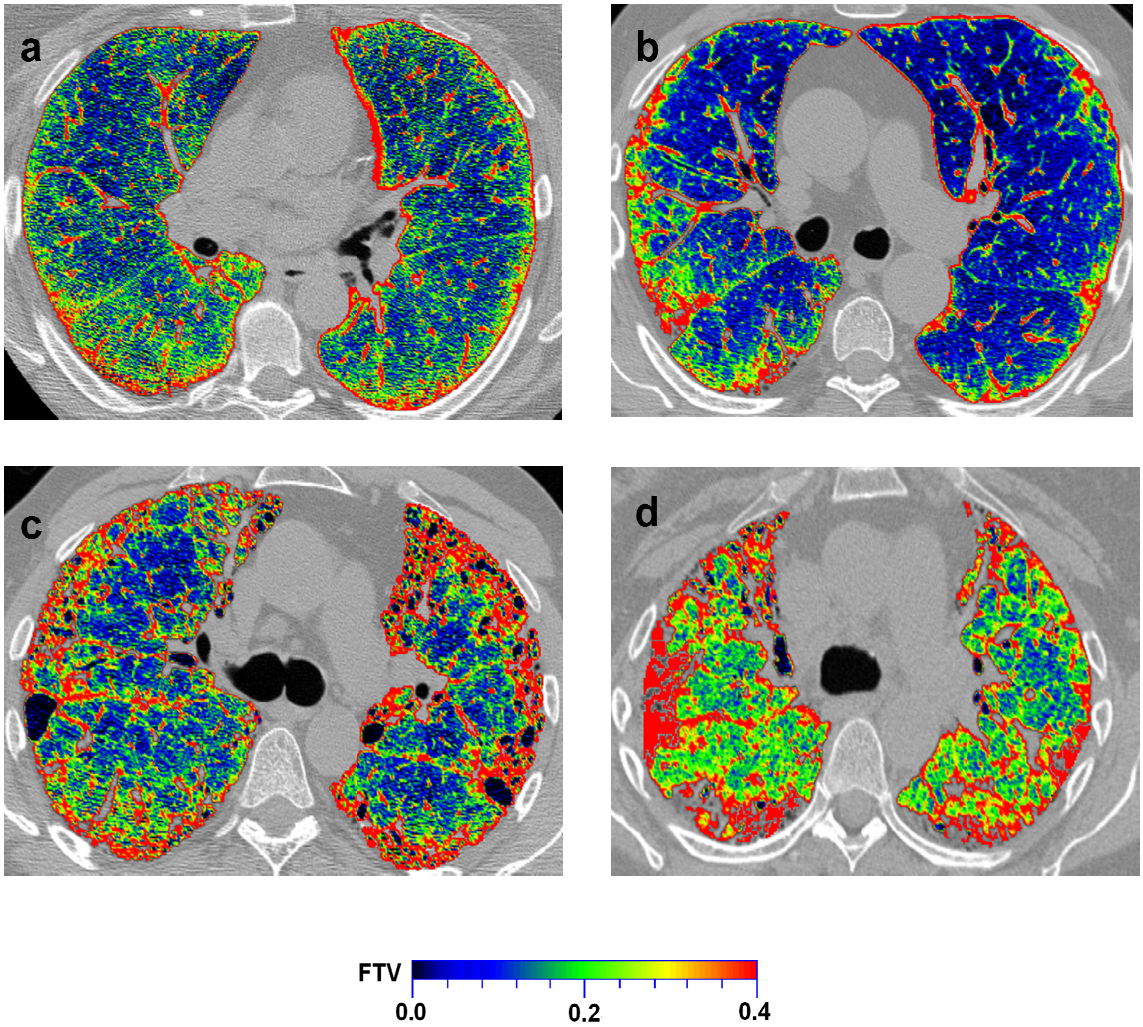

Figure 3.2 HRCT-derived surface color maps for FTV for (a) mild (b) moderate (c) severe and (d) more severe ILD. The high FTV regions in the color maps show the increase in FTV with increasing disease severity.

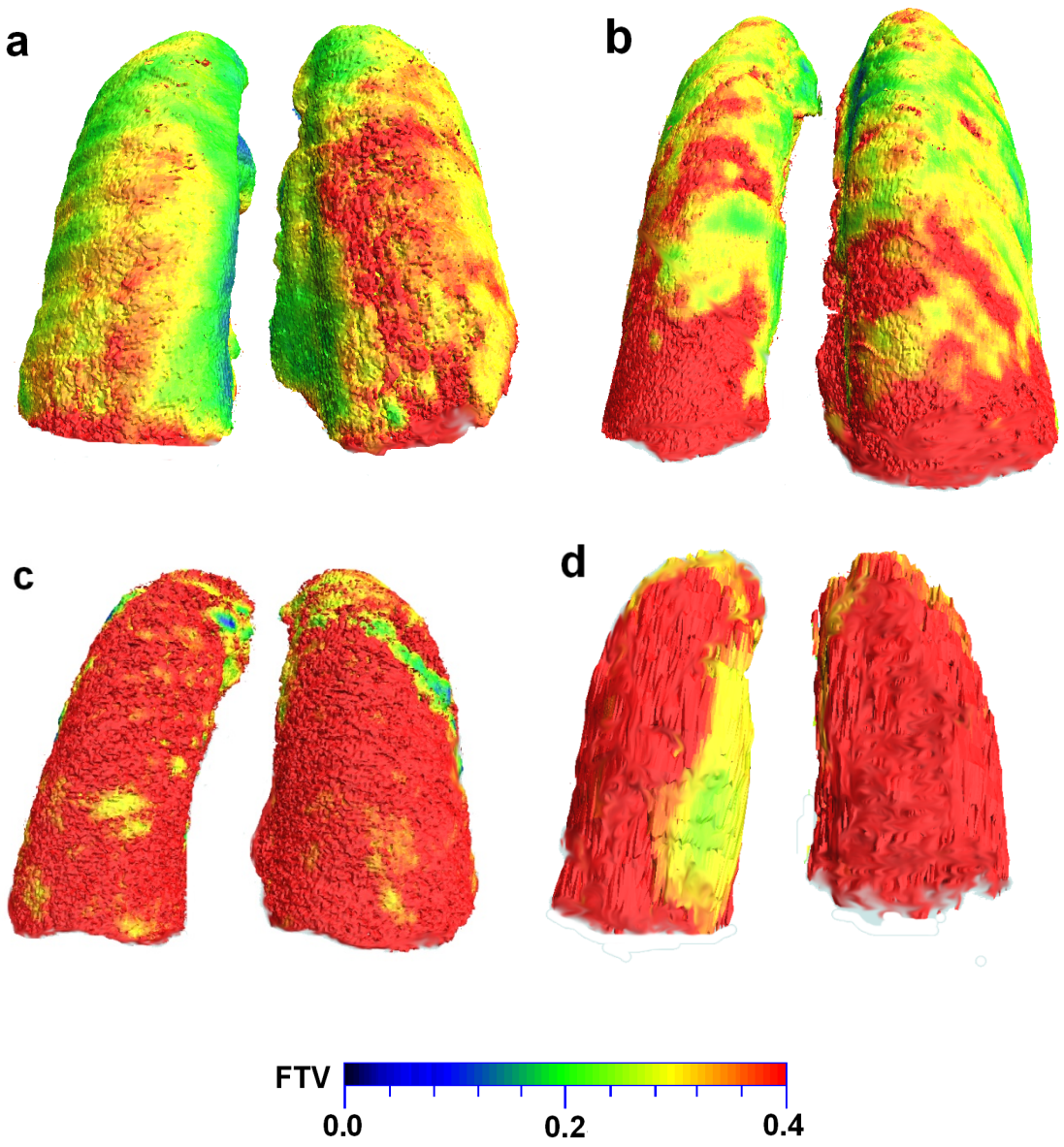

Figure 3.3 Three-dimensional surface color maps in FTV for (a) mild, (b) moderate, (c) severe and (d) more severe ILD. In early ILD lower lobes are affected, but with increasing disease severity middle and upper lobes are also affected. This can be seen by the regions of high FTV.

3.2 Quantitative analysis of CT

Absolute air and tissue volumes and FTV are summarized for each lobe: RUL, RML, RLL, LUL and LLL, each lung and both lungs in each posture and respiratory phase: supine end-expiration, supine end-inspiration and prone end-inspiration for each ILD group: mild, moderate, severe and more severe.

Air volumes are shown in Table 3.1. Air volume is lower in the lower lobes than upper lobes in all 3 inspiratory phases for each ILD group. In the mild, moderate and severe ILD groups the air volume was lower in the lower lobes than upper lobes in both right and left lungs. However, in the more severe ILD group there is no significant decrease in air volume in lower lobes compared to upper lobes. Total air volume in both lungs decreased with increasing disease severity in all positions, and it is also higher in supine end-inspiration and prone end-inspiration than supine end-expiration (Figure 3.4.a).

Absolute tissue volumes are shown in Table 3.2. Tissue volume is higher in lower lobes as compared to upper lobes in all inspiratory phases for each ILD group. Total tissue volume in both lungs increased with increasing disease severity from mild to severe ILD in all positions, and decreased in the more severe group (Figure 3.4.b).

The FTV is shown in Table 3. 3. FTV is significantly higher in right lower lobe than right upper lobe in supine end-inspiration, prone end-inspiration and supine end-expiration in all ILD groups. The FTV was significantly higher in left lower lobe than left upper lobe in the more severe ILD group at supine end-inspiration and in the severe ILD group at prone end-inspiration. Total FTV in both lungs increased with increasing disease severity in all positions, and it is also higher in supine end-expiration than other positions (Figure 3.4.c).

Table 3.1 Air volume (mL, mean±SD)

		Disease Severity																					
Position	**Lobe**	**Mild**					**Moderate**					**Severe**					**More Severe**							
		n=7					**n=11**					**n=9**					**n=2**							
SUP-EXP	**RUL**	559	±	267			391	±	215			307	±	153		*	86	±	15				*e
	RML	256	±	124	#		210	±	94	#		154	±	51	#	*	53	±	17				*§
	RLL	452	±	352	h		235	±	117	#	*	136	±	55	#	*	262	±	153				
	LUL	618	±	312			512	±	285			318	±	113		*	182	±	31				*
	LLL	422	±	241	¶		286	±	207	¶		169	±	97	¶	*	310	±	215				
	R Lung	1267	±	719			837	±	357		*	596	±	138		*	401	±	151				*
	L Lung	1041	±	549			797	±	455			487	±	179		*	492	±	246				
	Total	2308	±	1264			1634	±	631		b	1084	±	208		*	893	±	397				*
SUP-INSP	**RUL**	997	±	275			689	±	337		*	633	±	280		*	78	±	35				*§†
	RML	508	±	297	#		342	±	153	#	b	290	±	119	#	*	128	±	63				*
	RLL	967	±	601			521	±	248	‡	*	337	±	191	#	*	358	±	33				*
	LUL	1068	±	354			940	±	496			572	±	169		*§	265	±	80				*§
	LLL	903	±	459			654	±	447	i		408	±	224	¶	*	426	±	36				
	R Lung	2471	±	925			1552	±	569		*	1260	±	391		*	565	±	65				*§
	L Lung	1971	±	791			1594	±	839			980	±	308		*c	691	±	44				*
	Total	4442	±	1679			3146	±	1048		*	2239	±	568		*d	1256	±	109				*§
PRONE-INSP	**RUL**	906	±	331			596	±	315		a	642	±	281			125	±	15				*c†
	RML	339	±	121	#		303	±	137	#		266	±	135	#		63	±	22	g			*§f
	RLL	1112	±	630	‡		683	±	379	‡	a	348	±	178	#	*	373	±	154				*
	LUL	1069	±	407			868	±	521			676	±	201		b	224	±	3				*§
	LLL	1061	±	465			765	±	479			476	±	245	¶	*	440	±	159				b
	R Lung	2357	±	1049			1582	±	662		*	1256	±	366		*	560	±	117				*d
	L Lung	2130	±	796			1632	±	864			1153	±	401		*	663	±	156				*
	Total	4487	±	1808			3215	±	1130		*	2409	±	585		*	1224	±	273				*§

Mean±SD. * p<0.05 and a p=0.056 and b=0.06 vs. Mild; § p<0.05, c p=0.08 vs. Moderate; † p<0.05 and d=0.066 vs. Severe by factorial ANOVA. #p<0.05 and e p=0.05 g p=0.07vs. RUL; ‡ p<0.05 vs. RML; ¶ p<0.05 and h p=0.07 vs. LUL by repeated measures ANOVA.

Table 3.2 Tissue volume (mL, mean±SD)

		Disease Severity																			
Position	**Lobe**	**Mild**				**Moderate**				**Severe**					**More Severe**						
		n=7				**n=11**				**n=9**					**n=2**						
SUP-EXP	**RUL**	133	±	24		161	±	60		177	±	55			56	±	27		**b§†**		
	RML	59	±	13	**#**	78	±	24	**#**	88	±	31	**#**	*****	42	±	44		**†**		
	RLL	161	±	45	**g‡**	156	±	55	**‡**	168	±	66	**‡**		184	±	55	**‡**			
	LUL	152	±	35		196	±	34	*****	202	±	51		*****	107	±	49		**§†**		
	LLL	156	±	35		173	±	79		180	±	65			180	±	12				
	R Lung	353	±	71		395	±	107		433	±	126			282	±	127				
	L Lung	308	±	68		369	±	104		382	±	109			287	±	61				
	Total	661	±	137		765	±	191		815	±	224			570	±	187				
SUP-INSP	**RUL**	127	±	27		159	±	62		181	±	54		*****	44	±	29		**a §†**		
	RML	66	±	26	**#**	76	±	24	**#**	92	±	34	**#**		76	±	71				
	RLL	171	±	37	**#‡**	167	±	59	**‡**	172	±	66	**‡**		205	±	83	**‡**			
	LUL	145	±	42		193	±	33	*****	195	±	55		*****	128	±	73		**cd**		
	LLL	158	±	36		178	±	84	*****	192	±	64		*****	200	±	61	**h**	***§**		
	R Lung	364	±	57		402	±	113		446	±	127			324	±	182				
	L Lung	303	±	75		371	±	110		387	±	109			328	±	135				
	Total	667	±	126		773	±	209		833	±	230			652	±	317				
PRONE-INSP	**RUL**	120	±	37		152	±	57		178	±	60		*****	77	±	45		**†**		
	RML	54	±	12	**#**	78	±	24	**#**	96	±	46	**#**	*****	41	±	42	**e**	**†**		
	RLL	160	±	38	**#‡**	173	±	69	**‡**	155	±	57	**‡**		175	±	54	**#‡**			
	LUL	150	±	44		193	±	43		213	±	63		*****	112	±	55		**†**		
	LLL	152	±	34		182	±	97		178	±	59	**¶**		176	±	32				
	R Lung	333	±	78		403	±	117		429	±	127			293	±	141				
	L Lung	302	±	76		376	±	133		391	±	115			288	±	87				
	Total	635	±	147		779	±	241		820	±	236			581	±	228				

Mean±SD. * p<0.05 and a p=0.056 and b=0.06 vs. Mild; § p<0.05, c p=0.08 vs. Moderate; † p<0.05 and d=0.066 vs. Severe by factorial ANOVA. #p<0.05 and e p=0.05 g p=0.07vs. RUL; ‡ p<0.05 vs. RML; ¶ p<0.05 and h p=0.07 vs. LUL by repeated measures ANOVA.

Table 3.3 FTV (mean±SD)

		Disease Severity																				
Position	**Lobe**	**Mild**				**Moderate**				**Severe**				**More Severe**								
		n=7				**n=11**				**n=9**				**n=2**								
SUP-EXP	**RUL**	0.210	±	0.062		0.314	±	0.080		*	0.380	±	0.072		*d	0.387	±	0.159			*	
	RML	0.202	±	0.053		0.289	±	0.071	#	*	0.368	±	0.088		*§	0.369	±	0.225			*	
	RLL	0.302	±	0.078	#‡	0.415	±	0.105	#‡	*	0.553	±	0.079	#‡	*§	0.437	±	0.220	‡			
	LUL	0.213	±	0.057		0.308	±	0.095		*	0.401	±	0.108		*§	0.366	±	0.146			a	
	LLL	0.288	±	0.054	¶	0.418	±	0.128	¶	*	0.536	±	0.136	¶	*§	0.407	±	0.193				
	R Lung	0.238	±	0.057		0.333	±	0.072		*	0.419	±	0.075		*§	0.417	±	0.200			*	
	L Lung	0.244	±	0.053		0.348	±	0.106		*	0.448	±	0.120		*§	0.389	±	0.170				
	Total	0.241	±	0.055		0.333	±	0.083		*	0.427	±	0.088		*§	0.403	±	0.186			*	
SUP-INSP	**RUL**	0.118	±	0.032		0.204	±	0.068		*	0.236	±	0.066		*	0.344	±	0.054			*§†	
	RML	0.127	±	0.037	e	0.200	±	0.063		*	0.255	±	0.086		*	0.329	±	0.133			*§	
	RLL	0.177	±	0.065	‡	0.256	±	0.066	#‡	*	0.361	±	0.088	#‡	*§	0.359	±	0.116			*	
	LUL	0.122	±	0.026		0.191	±	0.064		*	0.265	±	0.085		*§	0.313	±	0.064			*§	
	LLL	0.163	±	0.045	¶	0.251	±	0.087	¶	a	0.350	±	0.116	¶	*§	0.318	±	0.085			*	
	R Lung	0.136	±	0.029		0.215	±	0.053		*	0.268	±	0.070		*	0.350	±	0.108			*§	
	L Lung	0.139	±	0.026		0.211	±	0.068		*	0.294	±	0.094		*§	0.315	±	0.077			*c	
	Total	0.137	±	0.028		0.206	±	0.055		*	0.276	±	0.075		*§	0.331	±	0.092			*§	
PRONE-INSP	**RUL**	0.122	±	0.034		0.229	±	0.101		*	0.226	±	0.052		*	0.364	±	0.116			*§†	
	RML	0.143	±	0.036	#	0.230	±	0.094		b	0.274	±	0.085		*	0.336	±	0.196			*	
	RLL	0.140	±	0.039		0.220	±	0.058		*	0.325	±	0.073	#‡	*§	0.334	±	0.159			*§	
	LUL	0.128	±	0.028		0.206	±	0.072		*	0.246	±	0.070		*	0.324	±	0.109			*§	
	LLL	0.132	±	0.024		0.220	±	0.072		*	0.298	±	0.101	f	*§	0.298	±	0.113	f		*	
	R Lung	0.133	±	0.032		0.219	±	0.071		*	0.257	±	0.053		*	0.341	±	0.156			*§	
	L Lung	0.128	±	0.021		0.205	±	0.063		*	0.262	±	0.077		*d	0.307	±	0.114			*c	
	Total	0.130	±	0.026		0.206	±	0.064		*	0.256	±	0.058		*	0.324	±	0.134			*§	

Mean±SD. * p<0.05 vs. Mild; § p<0.05 vs. Moderate by factorial ANOVA. #p<0.05 and e p=0.07vs. RUL; ‡ p<0.05 vs. RML; ¶ p<0.05 and f p=0.07 vs. LUL by repeated measures ANOVA

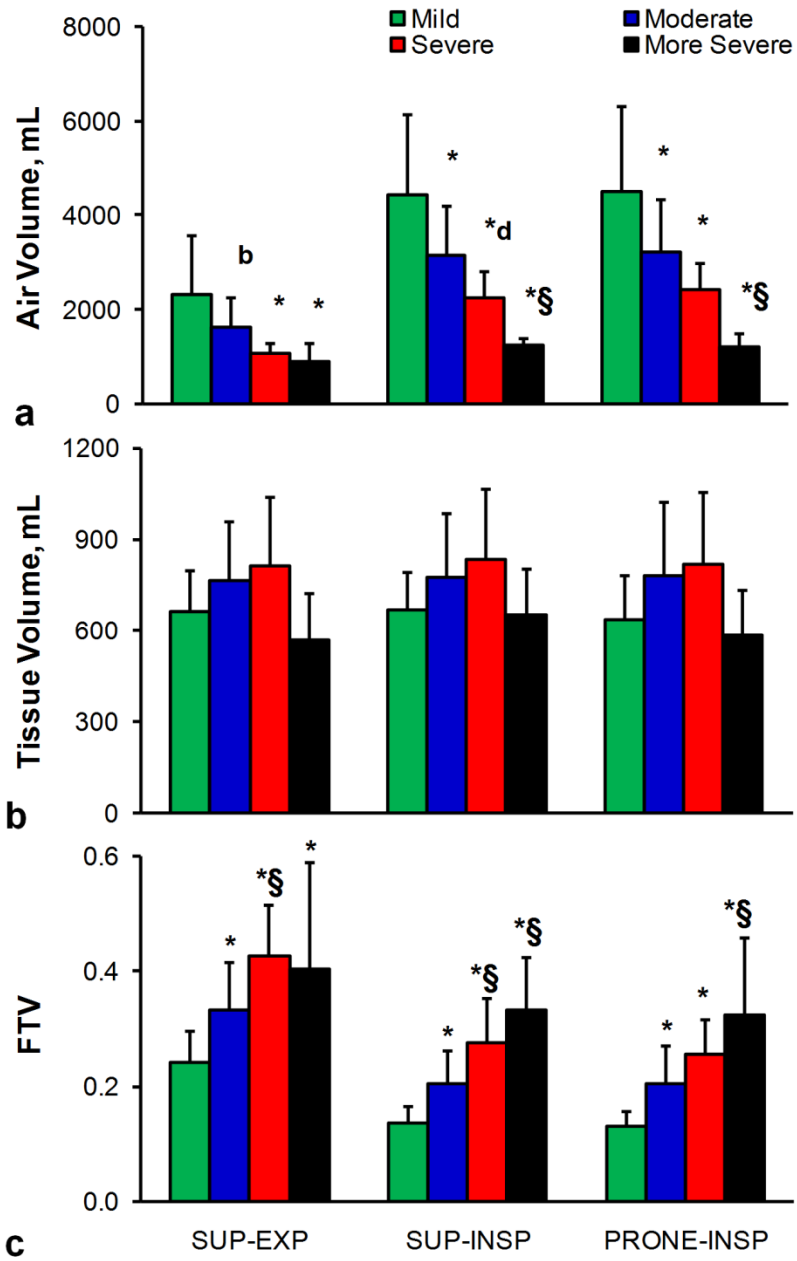

Figure 3.4 (a)Total air volume , (b) tissue volume and (c) FTV in both lungs are shown at supine-expiration (SUP-EXP), supine-inspiration (SUP-INSP) and prone-inspiration (PRONE-INSP) position within the four ILD groups: mild, moderate, severe and more severe. * $p<0.05$ and **b**=0.08 vs. mild; **§** $p<0.05$ **d** $p=0.08$ vs. moderate by factorial ANOVA.

3.3 FTV distribution within individual lobes

Intra-lobar distribution of FTV at prone end-inspiration is shown along each coordinate axis in Figure 3.5. Significant intra-lobar FTV gradients were observed in all lobes, with larger magnitudes and gradients in upper lobes than middle or lower lobes. Early ILD is associated with patchy tissue distribution mostly in the lower lobes. Regional FTV increased with ILD severity; absolute FTV was higher especially at the periphery of the lobes along medial-to-lateral and posterior-to-anterior region.

3.4 Comparison of the coefficient of variation of FTV distribution within individual lobes

The coefficient of variation for FTV among lobes is shown in Figure 3.6 at prone end-inspiration for the right, left and both lungs along 3 axes. With increasing ILD severity the coefficient of variation of FTV declined in the cephalad-to-caudal direction in right, left and both lungs and in posterior-to-anterior direction in right lung. In the early ILD stage there is increase in non-homogeneous tissue distribution especially in the periphery of the lobes. This can be seen with higher coefficient of variation in FTV that determines heterogeneity in tissue density in the mild and moderate ILD stage. But in the later stage of ILD the fibrotic tissue is increased and almost the entire lung is affected which resulted in decreasing heterogeneity and in turn the coefficient of variation in FTV declines.

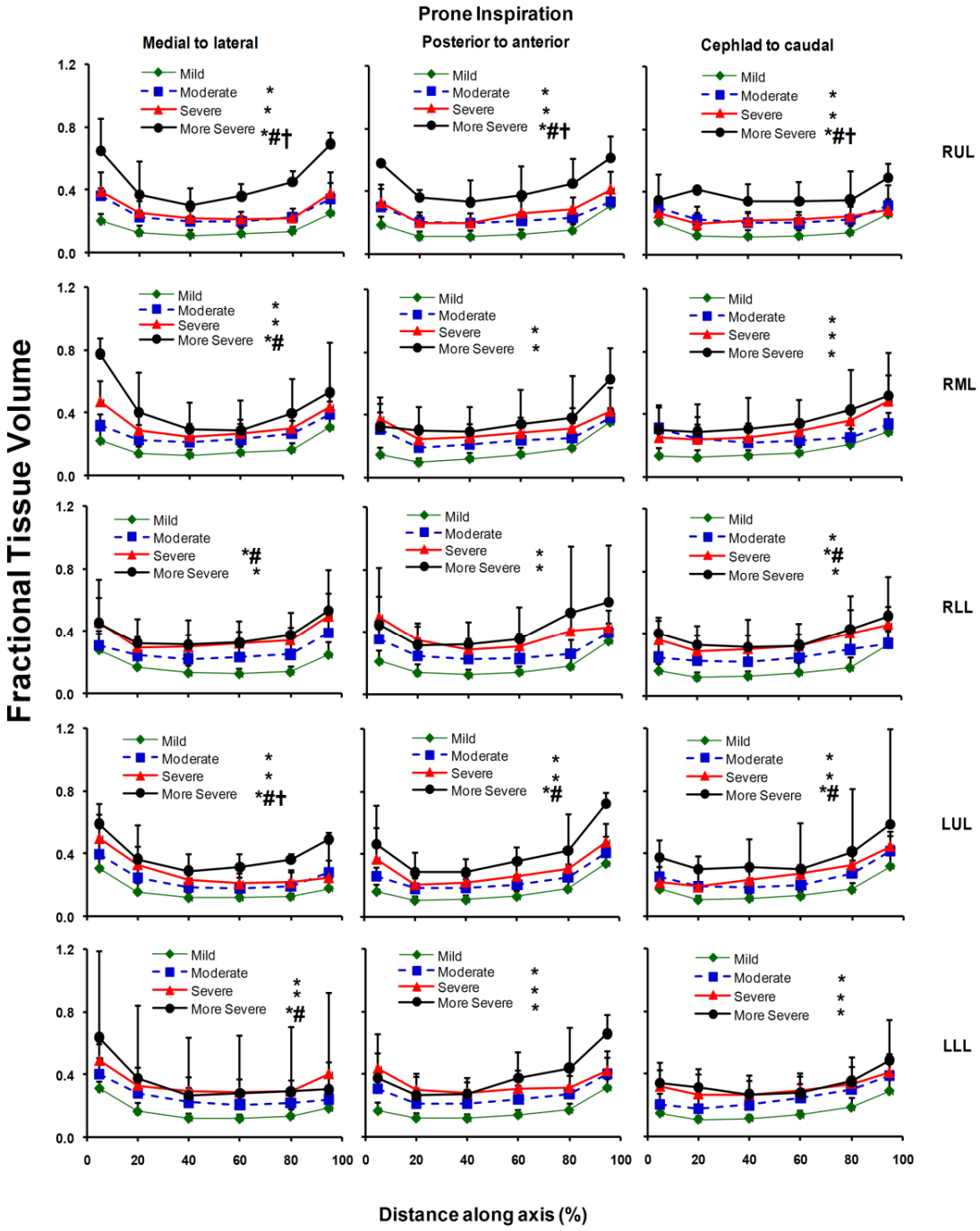

Figure 3.5 FTV distributions within individual lobes are shown in the prone end- inspiration position. Mean±SD. $p \leq 0.05$ * vs. mild, # vs. moderate, † vs. severe by repeated measures ANOVA.

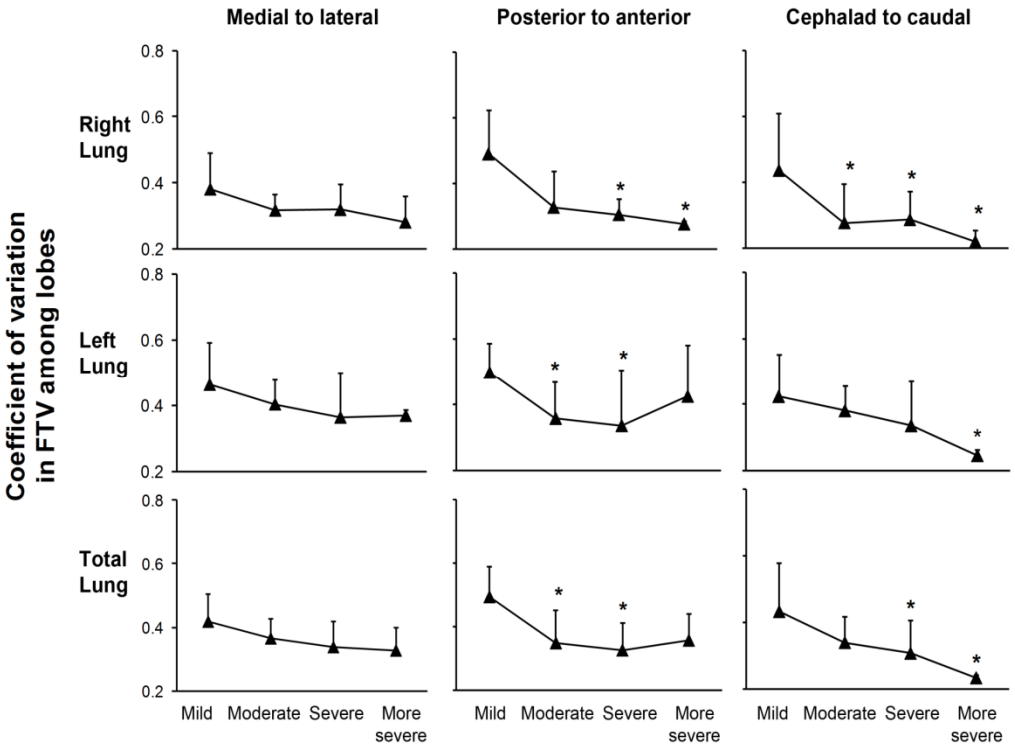

Figure 3.6 The coefficient of variation for FTV among lobes are shown in the prone-inspiratory position for right lung, left lung and both lungs along medial-to-lateral, posterior-to-anterior, cephalad-to-caudal axes * $p \leq 0.05$ vs. mild by ANOVA.

3.5 Correlation of CT-derived parameters with lung function

The correlation of air volume and tissue volume with lung function was not statistically significant due to low coefficient of correlation (R^2) values. However, in all lobes and all positions FTV correlated inversely with lung function parameters: FEV_1, FVC and DL_{CO} (all in % predicted), absolute FEV_1, FVC and DL_{CO} and transcutaneous O_2 saturation. FTV increases while lung function decreases with disease severity; hence FTV correlated inversely with lung function parameters. Table 3.4 shows the coefficient of correlation (R^2) values for correlation between FTV and lung function at supine end-expiration, supine end-inspiration and prone end-inspiration in each lobe.

Table 3.4 Coefficient of correlation (R^2) between FTV (Y-axis) and lung function parameters (X-axis).(*p< 0.05)

Position	Lobe	FEV_1 L	FEV_1 % predicted	FVC L	FVC % predicted	DL_{CO} (mL/mm/mmHg)	DL_{CO} % predicted	O_2 saturation fraction
SUPINE-EXPIRATION	**RUL**	0.34*	0.45*	0.37*	0.40*	0.28*	0.42*	0.44*
	RML	0.42*	0.46*	0.28*	0.42*	0.44*	0.50*	0.59*
	RLL	0.32*	0.40*	0.36*	0.37*	0.24*	0.31*	0.29*
	LUL	0.24*	0.32*	0.32*	0.34*	0.16*	0.22*	0.27*
	LLL	0.21*	0.24*	0.27*	0.25*	0.12	0.17*	0.13
SUPINE-INSPIRATION	**RUL**	0.36*	0.55*	0.40*	0.55*	0.34*	0.47*	0.25*
	RML	0.47*	0.55*	0.34*	0.52*	0.45*	0.48*	0.48*
	RLL	0.51*	0.55*	0.53*	0.52*	0.41*	0.45*	0.35*
	LUL	0.31*	0.45*	0.40*	0.53*	0.24*	0.29*	0.14
	LLL	0.39*	0.39*	0.44*	0.41*	0.28*	0.29*	0.20*
PRONE-INSPIRATION	**RUL**	0.28*	0.41*	0.29*	0.38*	0.28*	0.36*	0.21*
	RML	0.36*	0.46*	0.28*	0.38*	0.41*	0.43*	0.43*
	RLL	0.54*	0.67*	0.53*	0.60*	0.43*	0.46*	0.45*
	LUL	0.26*	0.41*	0.34*	0.47*	0.20*	0.23*	0.29*
	LLL	0.43*	0.48*	0.47*	0.47*	0.30*	0.31*	0.39*

Figure 3.7 shows correlation of FTV with lung function parameters: FEV_1, FVC and DL_{CO} (% predicted). FTV correlated inversely with FEV_1, FVC and DL_{CO} (all in % predicted) at supine end-expiration, supine end-inspiration and prone end-inspiration positions in (a) RUL, (b) RML, (c) RLL, (d) LUL and (e) LLL.

In RUL stronger correlations are observed at supine end-inspiration with respect to FEV_1 (R^2 =0.556), FVC (R^2 =0.552) and DL_{CO} (R^2 =0.470) (all in % predicted) than prone end-inspiration and supine end-expiration (Figure 3.7). Also in RML stronger correlations are observed at supine end-inspiration with respect to FEV_1 (R^2 =0.551), FVC (R^2 =0.524) and DL_{CO} (R^2 =0.487) (all in % predicted) than prone end-inspiration and supine end-expiration (Figure 3.8). In LUL stronger correlations are observed at supine end-inspiration with respect to FEV_1 (R^2 =0.458), FVC (R^2 =0.531) and DL_{CO} (R^2 =0.290) (all in % predicted) than prone end-inspiration and supine end-expiration (Figure 3.9). However in RLL stronger correlations were observed at prone end-inspiration with respect to FEV_1 (R^2 =0.551), FVC (R^2 =0.524) and DL_{CO} (R^2 =0.487) (all in % predicted) than supine end-inspiration and supine end-expiration (Figure 3.9). Also in LLL stronger correlations were observed at prone end-inspiration with respect to FEV_1 (R^2 =0.489), FVC (R^2 =0.472) and DL_{CO} (R^2 =0.317) (all in % predicted) than supine end-inspiration and supine end-expiration (Figure 3.11).

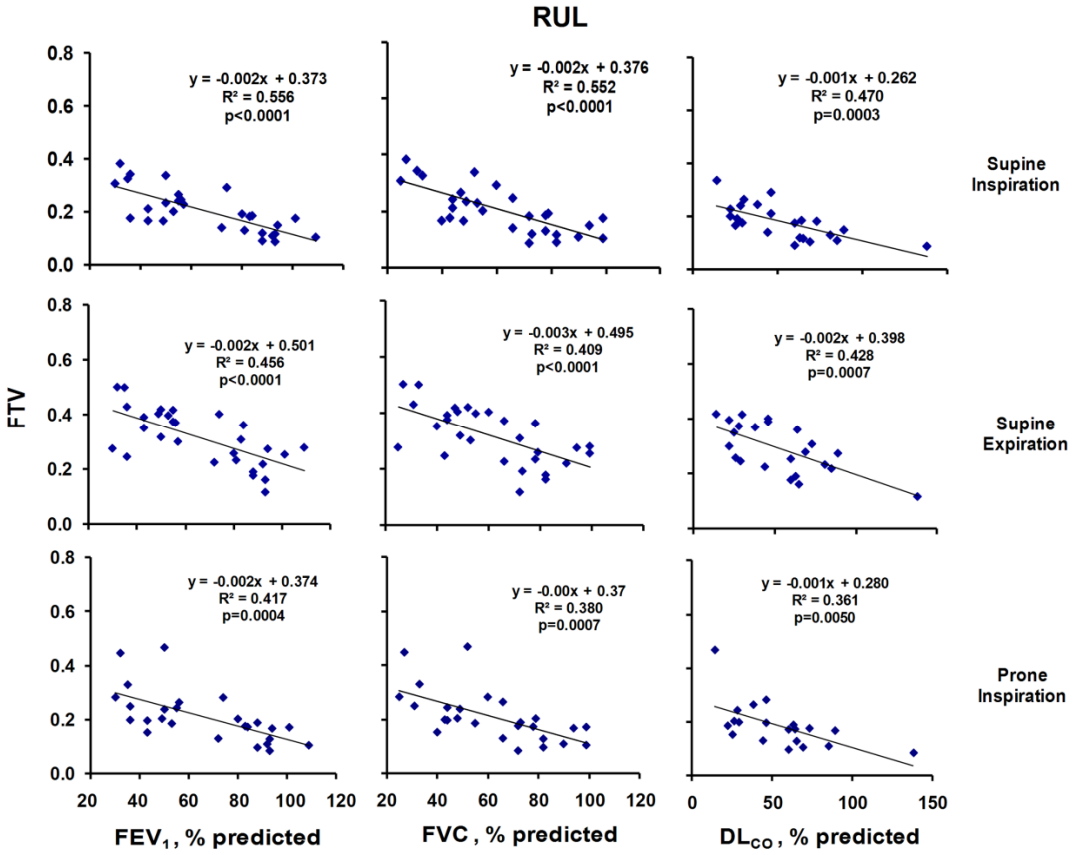

Figure 3.7 Correlation of FTV with lung function: FEV_1, FVC and DL_{CO} (% predicted) in RUL

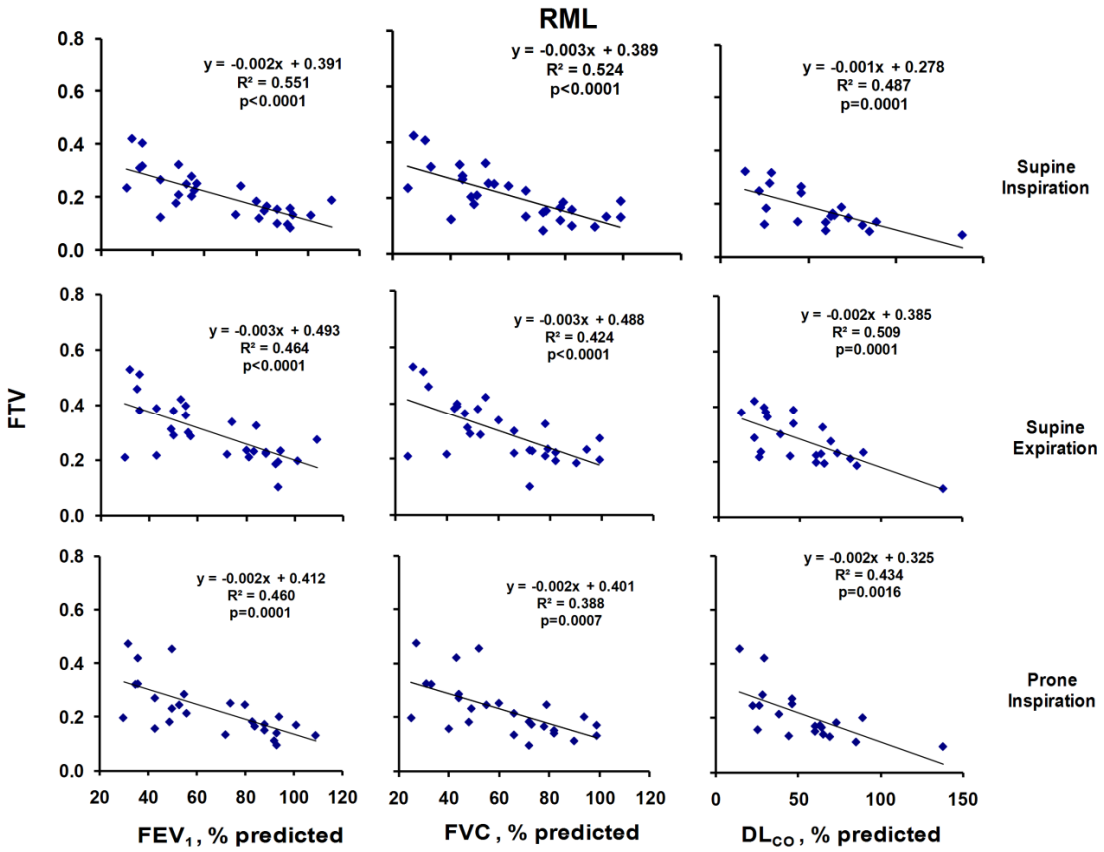

Figure 3.8 Correlation of FTV with lung function: FEV_1, FVC and DL_{CO} (% predicted) in RML

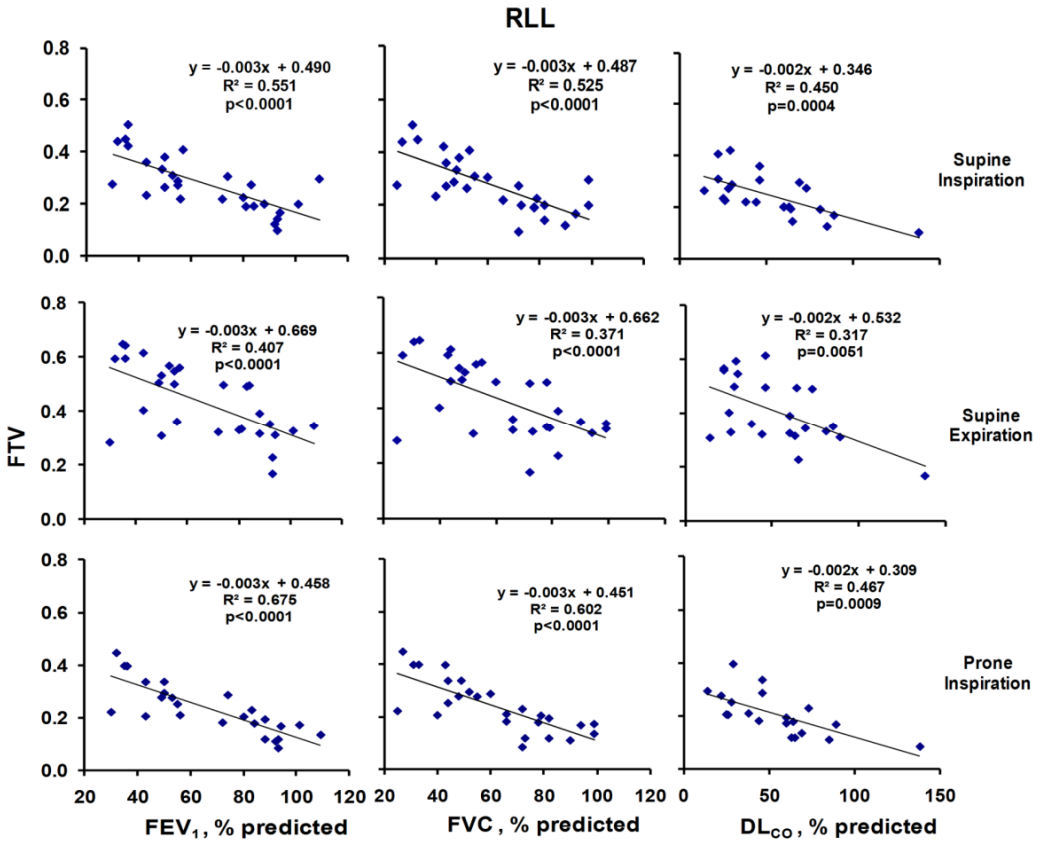

Figure 3.9 Correlation of FTV with lung function: FEV_1, FVC and DL_{CO} (% predicted) in RLL

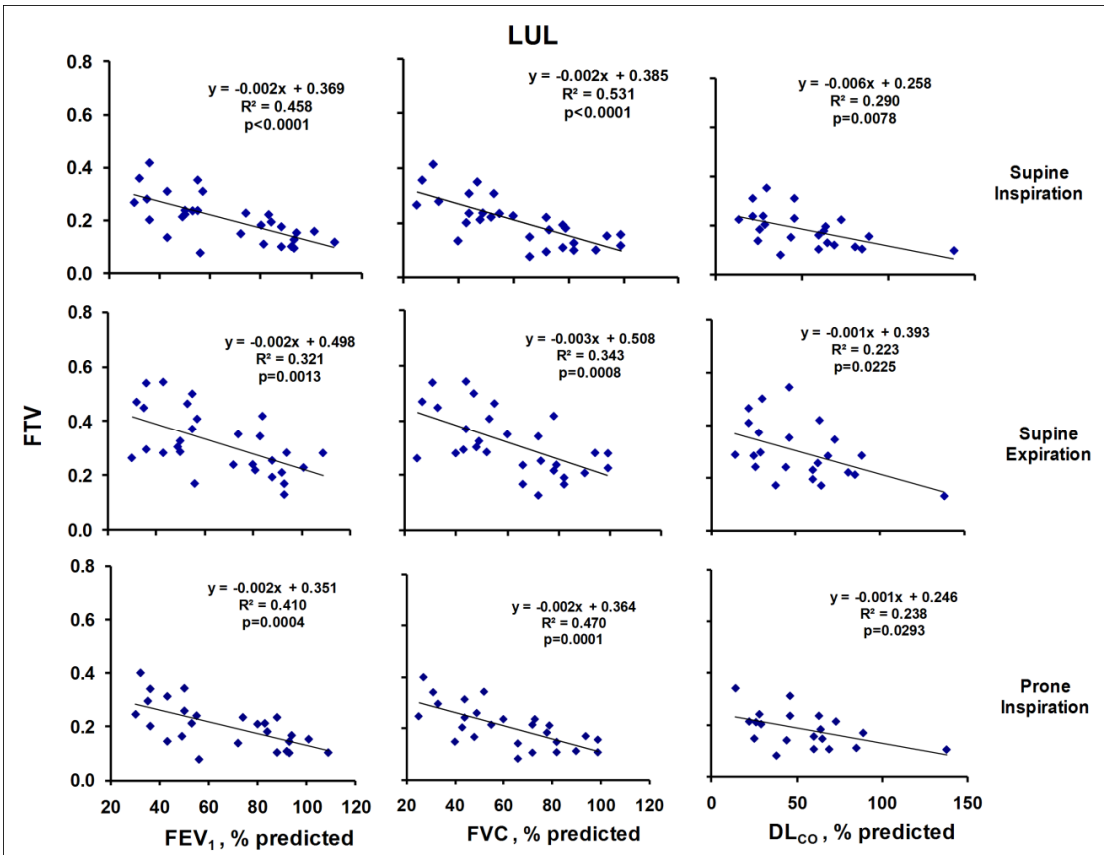

Figure 3.10 Correlation of FTV with lung function: FEV_1, FVC and DL_{CO} (% predicted) in LUL

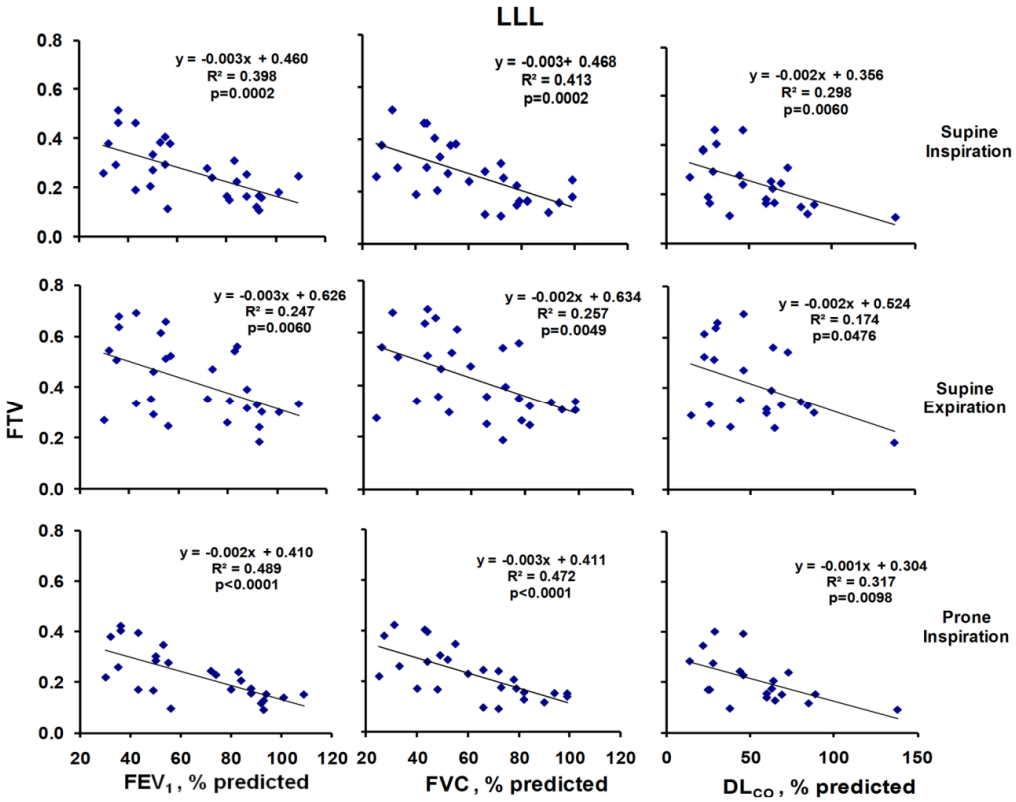

Figure 3.11 Correlation of FTV with lung function: FEV_1, FVC and DL_{CO} (% predicted) in LLL.

3.6 Correlation of intra-lobar coefficient of variation with lung function

The coefficient of variation of FTV within lobes, a marker of intra-lobar heterogeneity, correlated with FEV_1, FVC and DL_{CO} (% predicted). Typically ILD affects the lower lobes in the early stage of the disease. Hence stronger correlations with significant correlation coefficient (R^2) values were observed in lower lobes than upper lobes and in prone end-inspiration than supine end-expiration or supine end-inspiration. In supine end-inspiration and supine end-expiration positions the coefficient of variation in FTV correlated strongly with lung function only along the posterior-to-anterior region of RLL than LLL.

The coefficient of variation of FTV showed a direct correlation with lung function, i.e., intra-lobar heterogeneity decreased with increase in disease severity. In the early stage of disease, the periphery of the lobe is affected. But with the advancement of the disease the entire lobe is affected; hence heterogeneity within lobes decreases. Table 3.5 shows the correlation coefficient (R^2) values between intra-lobar coefficient of variation in FTV and lung function: FEV_1, FVC and DL_{CO} (all in % predicted), absolute FEV_1, FVC and DL_{CO} and O_2 saturation in RLL and LLL in all positions. Correlation coefficient (R^2) values are shown only in RLL and LLL, since coefficient of variation in FTV correlated strongly with lung function in lower lobes than upper lobes.

Table 3.5 Coefficient of correlation (R^2) between intra-lobar CV in FTV (Y-axis) and lung function (X-axis) (* $p < 0.05$)

Position	Lobe	Axis	FEV_1 L	FEV_1 % predicted	FVC L	FVC %predicted	DL_{CO} mL (mm/mmHg)$^{-1}$	DL_{CO} % predicted	O_2 saturation fraction
SUPINE-EXPIRATION	RLL	X	0.02	0.00	0.02	0.00	0.03	0.16	0.06
		Y	0.29*	0.24*	0.29*	0.15*	0.12	0.23*	0.52*
		Z	0.00	0.00	0.00	0.00	0.00	0.09	0.01
	LLL	X	0.00	0.01	0.00	0.03	0.01	0.00	0.04
		Y	0.13*	0.04	0.14	0.03	0.01	0.01	0.15*
		Z	0.09	0.07	0.06	0.04	0.01	0.02	0.00
SUPINE-INSPIRATION	RLL	X	0.06	0.05	0.07	0.03	0.22*	0.24*	0.08
		Y	0.36*	0.22*	0.35*	0.20*	0.38*	0.26*	0.46*
		Z	0.11	0.17*	0.08	0.07	0.17*	0.29*	0.06
	LLL	X	0.07	0.06	0.13	0.05	0.13	0.15	0.05
		Y	0.16*	0.07	0.19*	0.08	0.06	0.04	0.02
		Z	0.13	0.19*	0.16*	0.16*	0.26*	0.30*	0.00
PRONE-INSPIRATION	RLL	X	0.16*	0.26*	0.16*	0.22*	0.22*	0.19	0.10
		Y	0.42*	0.42*	0.40*	0.28*	0.54*	0.60*	0.27*
		Z	0.09	0.31*	0.06	0.25*	0.11	0.12	0.00
	LLL	X	0.22*	0.19*	0.28*	0.17*	0.27*	0.23*	0.37*
		Y	0.23*	0.17*	0.26*	0.11	0.50*	0.47*	0.38*
		Z	0.24*	0.40*	0.27*	0.36*	0.13	0.13	0.04

3.6.1 FEV_1 (% predicted)

The coefficient of variation of FTV within lobes correlated with FEV_1 (% predicted) along all coordinate axes (Figure 3.12). Significant correlations were observed in RLL and LLL along medial-to-lateral, posterior-to-anterior and cephalad-to-caudal axes, also in RUL along posterior-to-anterior and cephalad-to-caudal axes and in RML along posterior-to-anterior axis. Stronger correlation was observed in RML (R^2=0.45) and RLL (R^2=0.425) along posterior-to-anterior region than RUL and LUL.

3.6.2 FVC (% predicted)

The coefficient of variation of FTV within lobes correlated with FVC (% predicted) along all coordinate axes (Figure 3.13). Significant correlations were observed in RLL and LLL along medial-to-lateral, posterior-to-anterior and cephalad-to-caudal axes, also in RUL along posterior-to-anterior and cephalad-to-caudal axes and in RML along posterior-to-anterior axis. Stronger correlation was observed in RML (R^2=0.356) along posterior-to-anterior region than RLL and LLL.

3.6.3 DL_{CO} (% predicted)

The coefficient of variation of FTV within lobes correlated with DL_{CO} (% predicted) along all coordinate axes except in the cephalad-to-caudal axis (Figure 3.14). Significant correlations were observed in RLL and LLL and RML along medial-to-lateral and posterior-to-anterior axes, and in RUL along posterior-to-anterior axis. Stronger correlation was observed in RML (R^2=0.543), RLL (R^2=0.6) and LLL (R^2=0.478) along posterior-to-anterior region than RUL and LUL. Intra-lobar heterogeneity decreased with increase in disease severity.

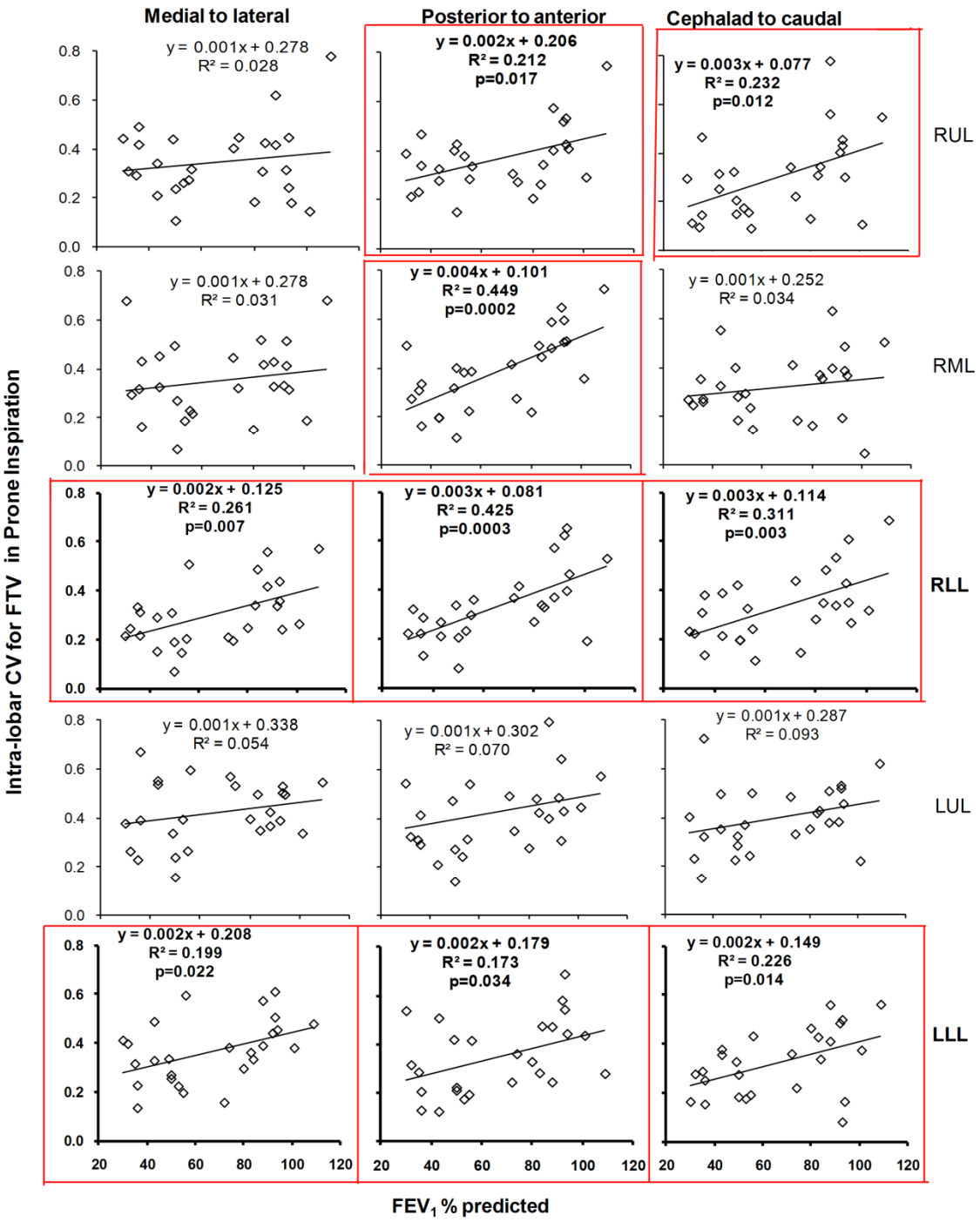

Figure 3.12 Correlation of the coefficient of variation in FTV within lobes along x (medial-to-lateral), y (posterior-to-anterior) and z (cephalad-to-caudal) axes at prone inspiration with FEV_1 (% predicted).Significant correlations of the coefficient of variation in FTV with FEV_1 (% predicted) are shown in red boxes.

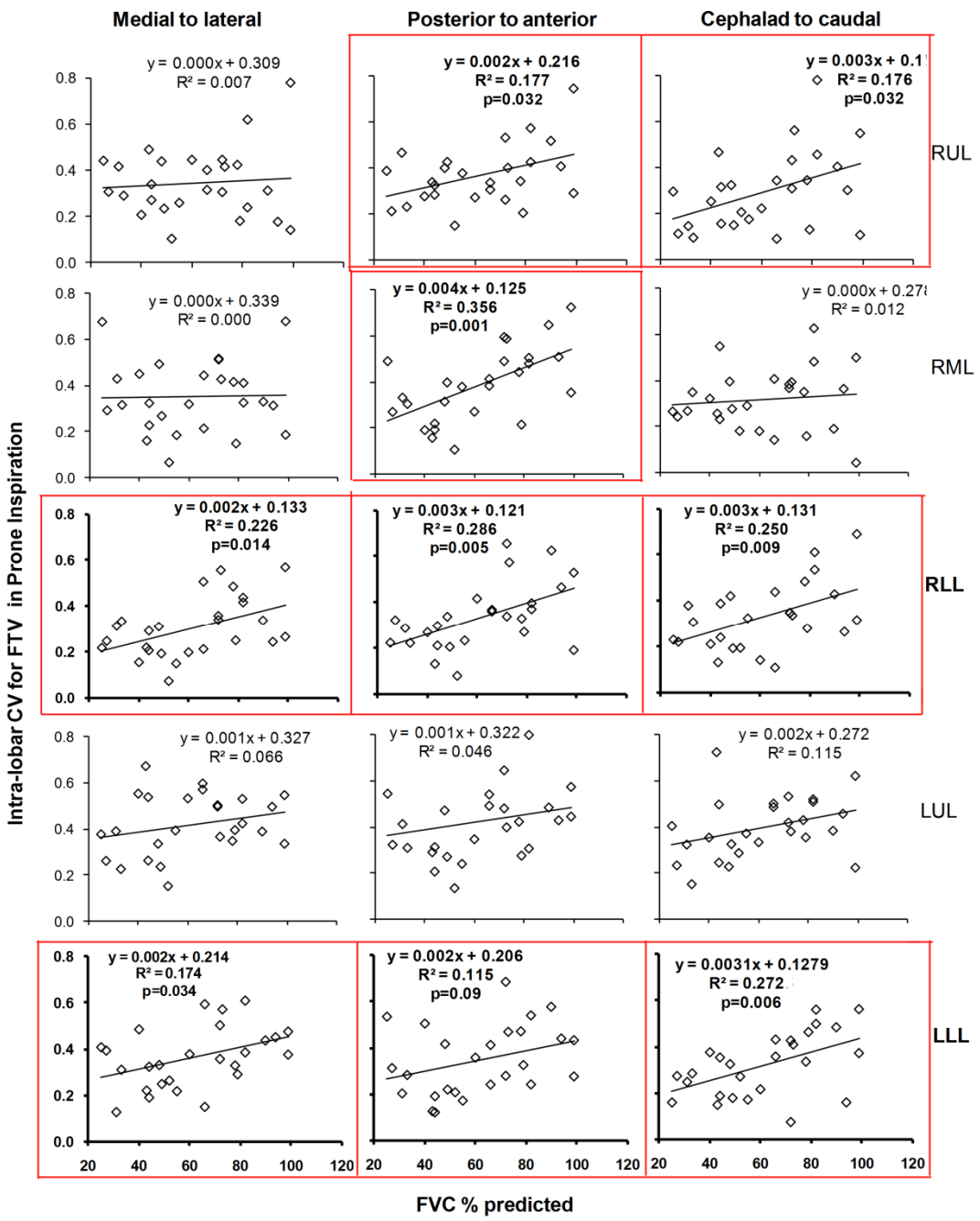

Figure 3.13 Correlation of the CV of FTV within lobes along x (medial-to-lateral), y (posterior-to-anterior) and z (cephalad-to-caudal) axes at prone inspiration with FVC (% predicted). Significant correlations of the coefficient of variation in FTV with FVC (% predicted) are shown in red boxes.

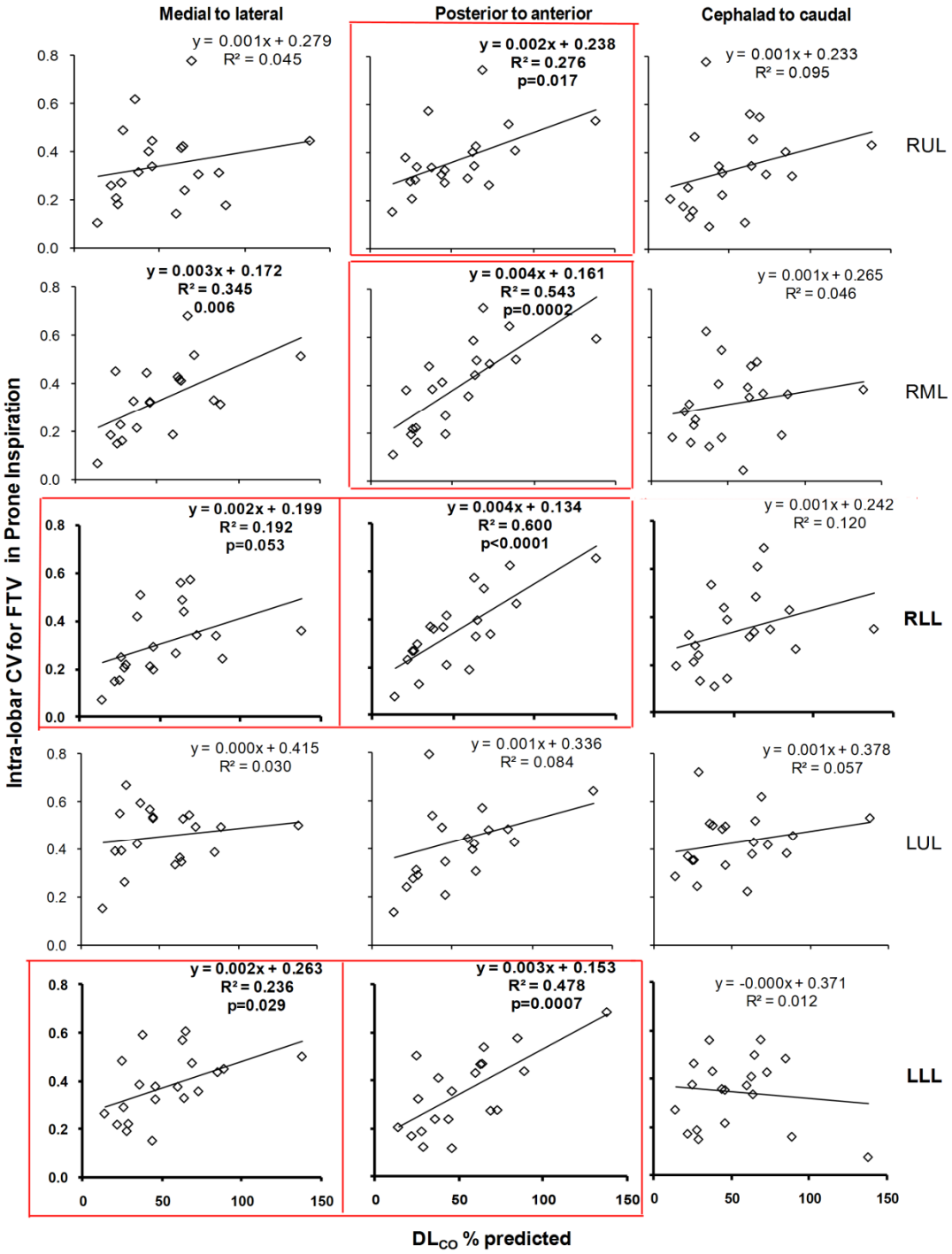

Figure 3.14 Correlation of the CV of FTV within lobes along x (medial-to-lateral), y (posterior-to-anterior) and z (cephalad-to-caudal) axes at prone inspiration with DL_{CO} (% predicted). Significant correlations of the coefficient of variation in FTV with DL_{CO} (% predicted) are shown in red boxes.

3.7 Correlation of inter-lobar coefficient of variation of FTV with lung function

Figure 3.15 shows correlation of Coefficient of Variation of FTV among lobes, a marker of inter-lobar heterogeneity, with FEV_1, FVC and DL_{CO} (all in % predicted) at supine end-expiration, supine end-inspiration and prone end-inspiration. The correlation of inter-lobar coefficient of variation of FTV with lung function was not significant with lower coefficient of correlation (R^2) values at supine end-expiration, supine end-inspiration. However, in the prone end-inspiration position, the coefficient of variation in FTV among lobes showed a modest inverse correlation with DL_{CO} ($p=0.05$). Inter-lobar heterogeneity increased with increasing disease severity. This can be explained by the fact that the lower and middle lobes are more affected than the upper lobes and the disparity becomes greater with increasing disease severity.

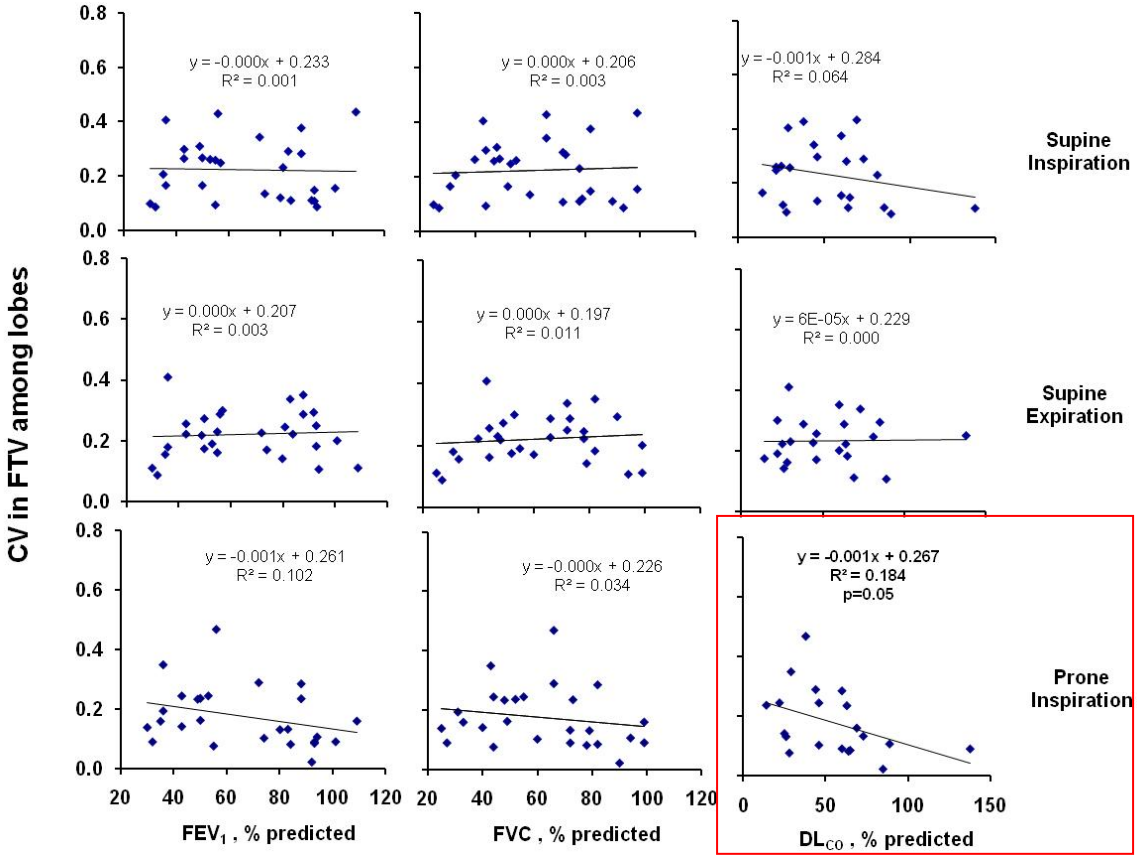

Figure 3.15 Correlation of the CV in FTV among lobes with lung function: FEV_1, FVC and DL_{CO} (% predicted). The coefficient of variation in FTV among lobes showed a significant modest inverse correlation with DL_{CO} (red box).

CHAPTER 4

DISCUSSION AND CONCLUSIONS

4.1 Literature review

Previously density-based lobar detection programs have been developed for quantification of ILD. In these studies a computer algorithm was used for semi-automatic delineation of the lobes with manual correction and the results were compared with visual scoring of ILD [24] [25]. These studies improved the qualitative analysis of ILD with computer assistance and minimal user intervention; but lacked quantitative analysis. Owing to the limitations of the qualitative studies, computer based CT quantitative studies were developed. Studies involved use of PC based software to isolate the lung parenchyma from the thoracic wall on thin-section CT scans. By applying automated computer thresholding technique, density threshold values were used to calculate CT derived parameters such as mean lung density. It has been shown that mean lung density is higher in idiopathic pulmonary fibrosis than in normal subjects. Also studies have quantified the lung density histogram. It has been shown that histogram shifts towards higher densities in idiopathic pulmonary fibrosis than in normal subjects [26] [27] [28]. In these studies quantitative CT indexes were calculated for the entire lung in every patient allowing global estimation of ILD but no attempt was made to quantify regional abnormalities in the lung. Other studies involved data from multiple centers. Images were segmented into regions using computer based program and density thresholding technique was used to calculate mean lung attenuation. These studies have raised questions of inter-scanner variability including differing CT calibrations. The attenuation (HU) measurements

vary due to beam hardening artifacts and change in lung volumes hence accurate comparison of results among different centers is difficult [29] [30].

4.2 Significance of the present study

We have described a quantitative voxel-wise method to map and analyze regional CT-derived parameters and to correlate quantitative anatomical data with lung function in patients with ILD. In this study we used natural boundaries to divide lungs into lobes, allowing comparisons within and among lobes and in three different postures. CT attenuation values for each voxel within each lobe are utilized to derive regional air volume, tissue volume and FTV expressed along standard coordinate axes. This method allows the comparison of lobar changes in attenuation even in the presence of anatomical distortion. The CT attenuation values were calibrated with respect to thoracic air and muscle in each subject to obtain tissue volume; hence data from different scanner models and multiple centers could be standardized for quantitative analysis of ILD. We also expressed the regional heterogeneity of as the CV of a given parameter. These CT-derived parameters and their respective CV's were correlated with clinical lung function measurements. This novel analysis technique is shown to be feasible and provides quantitative regional assessment of parenchymal abnormalities. This objective and quantitative approach can assist radiologists and pulmonary physicians to perform follow-up examinations from across different centers.

4.3 Summary of major findings

The major findings are as follows: 1) FTV increases with increasing ILD severity especially in the periphery. 2) FTV in all lobes correlated inversely with FEV_1, FVC and DL_{CO} in supine end-expiration, supine end-inspiration and prone end-inspiration positions. 3) Intra-lobar CV of FTV correlated with FEV_1, FVC and DL_{CO} only in the prone end-inspiration position and not in supine end-inspiration and supine end-expiration position. 4) With increasing ILD severity, FTV heterogeneity within lobes decreased especially in the lower lobes

while FTV heterogeneity among lobes increases. 5) HRCT images in ILD may be obtained and analyzed at larger intervals (6.25 mm apart) without loss of quantitative information.

We conclude that quantitative analysis of CT derived parameters provides clinically relevant markers of regional ILD. Increasing inter-lobar and decreasing intra-lobar heterogeneity developed with advancing ILD severity; these parameters are best assessed at prone end-inspiration.

4.4 Limitations of the study

In this study, the primary data set was collected from different centers that used different CT scanners. Although standard protocols were employed by all centers, differences in equipment performance may persist. The number of patients in the "more severe" ILD group was small (n=2). Demographic data were incomplete (e.g., DL_{CO} was not available in some patients). HRCT in the prone end-position was not available for 3 patients. The end-inspiration and end-expiration levels were not objectively verified by respiratory pressure, which might have resulted in variable inspiration and expiration volumes.

The semi-automatic analysis program had limitations in boundary detection. Since the program uses density thresholding to isolate the area occupied by the lung on the CT scan, due to patchy tissue distribution especially at the periphery of the lung, the pleural boundary were delineated manually, which might have resulted in error in area selection for the lobes. The tissue volume included the blood vessels and microvascular blood; hence the parenchymal tissue and microvascular blood could not be differentiated. Although this technique can detect regional changes of lung attenuation with disease severity, it is unable to distinguish the textural or patterning abnormalities such as ground glass opacity, reticular infiltrates and honeycombing. Texture based methods such as adaptive multiple feature and fractal analysis are being developed to identify and quantify these abnormal patterns [31] [32].

4.5 Future work

The data from this study can be used for future studies to follow longitudinal disease progression and response to treatment in patients with ILD. This analysis technique can be extended for studying other diffuse lung diseases such as emphysema that cause uneven lobar distortion. This analysis can also be extended to examine the diagnostic yield of conventional CT images in lung disease, which involves a lower radiation dose.

REFERENCES

[1] Carr J, Brown J. Introduction to biomedical equipment technology. The human respiratory system and its measurement. Singapore: Pearson Education, Inc, 2005: 323-344.

[2] Silverthorn, Dee Unglaub. Human Physiology: an integrated approach. Respiratory physiology. New Jersey: Prentice Hall, 1998:474-477.

[3] Stuart I. Fox. Biopac Manual. Measurements of pulmonary function . New York: Mac Graw-Hill, 2008:1-3.

[4] Armstrong P, Wilson A, Dee P, Hansell D. Imaging of Diseases of Chest. Diffuse interstitial lung disease. London, Harcourt Publishers Limited, 2000: 533-535.

[5] Dempsey, O.J., Clinical review: idiopathic pulmonary fibrosis--past, present and future, Respir Med, 2006. 100(11): p. 1871-85.

[6] Raghu G, Brown K. Interstitial lung disease: Clinical evaluation and keys to an accurate diagnosis. Clin Chest Med. 25: 2004: 409-419.

[7] Martinez, F.J. and K. Flaherty, Pulmonary function testing in idiopathic interstitial pneumonias. Proc Am Thorac Soc, 2006. 3(4): 315-21.

[8] American Thoracic Society. Single breath carbon monoxide diffusing capacity (transfer factor): recommendations for a standard technique¬1995 update. Am J Respir Crit Care Med 1995; 152; 2185-2198.

[9] Suetens P. Fundamental of Medical Imaging.Cambridge.X-ray computed tomography. UK, Cambridge University Press, 2002:66-69.

[10] Haaga J, Lanzeieri C, Gilkeson R. CT amd MR imaging of the whole body. Imaging principles in computed tomography. Missouri, Mosby Inc, 2003: 8-13.

[11] Hsieh, J,. Computed tomography principles, design, artifacts and recent advances. Major components of CT scanner. Washington, SPIE press, 2002: 147-150.

[12] Appoloni C, "Ceramic foams porous microstructure characterization by X-ray microtomography", Mat. Res. vol.7 no.4 São Carlos Oct./Dec. 2004.

[13] Hofer M, CT Teaching Manual. Physical and technical fundamentals.New York, Georg Thieme Verlag, 2007: 6-12.

[14] Webb R, Muller N, Naidich D, High-Resolution CT of the Lung. Technical Aspects of HRCT. Philadelphia, Lippincott Williams &Wilkins, 2001: 1-9.

[15] Hartley, P.G., et al., High-resolution CT-derived measures of lung density are valid indexes of interstitial lung disease. J Appl Physiol, 1994. 76(1): 271-7.

[16] Brantly M ,et.al. Pulmonary function and High-Resolution CT findings in patients with an inherited form of pulmonary fibrosis, Hermansky-Pudlak Syndrome, due to mutations in HPS-1*. Chest 2000; 117; 129-136.

[17] Mahesh M. Search for isotropic resolution in CT from conventional through multiple-row detector.RadioGraphics , 2002: 22:949–962.

[18] Fraser, Colman, Muller, Pare. Synopsis of Diseases of the Chest.Chronic interstitial lung disease. Philadelphia, Elsevier Saunders, 2005:449-455.

[19] Lynch D, Quantitative CT of Fibrotic Interstitial Lung Disease, Chest 2007;131: 643-644

[20] Ravikumar, P., et al., Regional lung growth following pneumonectomy assessed by computed tomography. J Appl Physiol, 2004. 97(4): 1567-74; discussion 1549

[21] Ravikumar P, Yilmaz C, Dane DM, Johnson RL, Jr.,Estera AS, and Hsia CC, Developmental signals do not further accentuate nonuniform postpneumonectomy compensatory lung growth, J Appl Physiol, 2007,102: 1170-1177

[22] Yilmaz C, P Ravikumar, DM Dane, DJ Bellotto, RL Johnson Jr., CCW Hsia. Non-invasive quantification of heterogeneous lung growth following extensive lung resection by high resolution computed tomography. J Appl Physiol, 2009 107:1569-1578.

[23] US department of Health & Human services, National Heart Lung and Blood Institute website.

[24] Revel, M.P., et al. Automated lobar quantification of emphysema in patients with severe COPD. Eur Radiol, 2008. 18(12): 2723-30.

[25] Zavaletta, V.A., B.J. Bartholmai, and R.A. Robb, High resolution multidetector CT-aided tissue analysis and quantification of lung fibrosis. Acad Radiol, 2007. 14(7): 772-87.

[26] Hoffman E, et al. Characterization of the interstitial lung diseases via density-based and texture- based analysis of computed tomography images of lung structure and function. Acad Radiol 2003; 10:1104-1118.

[27] Lamers R, et al. Reproducibility of spirometrically controlled CT lung densitometry in a clinical setting. Eur Respir J 1998; 11:942-945.

[28] Kalender WA, Fichete H, Bautz W, Skalej M.Semiautomatic evaluation procedures for quantitative CT of the lung. J Comput Assist Tomogr 1991;15: 248-255.

[29] Camiciottoli G, Orlandi I, Bartolucci M, et al. Lung CT densitometry in systemic sclerosis, correlation with lung function, exercise test and quality of life. Chest 2007; 131:672–681.

[30] Best AC, Lynch AM, Bozic CM, et al. Quantitative CT indexes in idiopathic pulmonary fibrosis: relationship with physiologic impairment. Radiology 2003; 228:407–414.

[31] Rodriguez LH, Vargas PF, Raff U, et al.Automated discrimination and quantification of idiopathic pulmonary fibrosis from normal lung parenchyma using generalized fractal dimensions in high resolution computed tomography images. Acad Radiol 1995; 2:10–18.

[32] Uppaluri R, Hoffman EA, Sonka M, et al.Interstitial lung disease: a quantitative study using the adaptive multiple feature method. Am J Respir Crit Care Med 1999; 159:519–525.

BIOGRAPHICAL INFORMATION

Snehal Watharkar was born and brought up in, India. She earned her Bachelor of Engineering degree in June 2007 from the University of Pune, India. Right after her bachelor's she took up graduate studies from the joint program in Biomedical Engineering at the University of Texas at Arlington and University of Texas Southwestern Medical Center at Dallas commencing in fall 2007. She plans to join the medical device industry with aims to extending her curriculum and research expertise to real-world clinical applications.